

**Re-Os geochronology of the Monterey Formation, Union Leroy  
51-18 well, Santa Maria Basin, California**

**A Thesis Presented to the  
Faculty of the Department of Earth and  
Atmospheric Sciences  
University of Houston**

**In Partial Fulfillment  
Of the requirements of the Degree  
Master of Science**

**By**

**Clint Barnette**

**August 2015**

**Re-Os geochronology of the Monterey Formation, Union Leroy  
51-18 well, Santa Maria Basin, California**

---

**Clint Barnette**

**Approved:**

---

**Dr. Alan Brandon**

---

**Dr. Joseph Curiale**

---

**Dr. Qi Fu**

---

**Dr. Steven Bergman**

---

**Dean, College of Natural Sciences and Mathematics**

## **Acknowledgements**

I'd like to thank my advisor and committee chair, Dr. Alan Brandon, for his support and constructive feedback throughout this Master's program and especially in relation to this thesis. I'd also like to thank my committee members, Dr. Joseph Curiale, Dr. Qi Fu, and Dr. Steven Bergman for their guidance through this project as well.

Thanks also go out to my family and friends for their support during my time at the University of Houston, and to the faculty and staff for helping develop me as a scientist.

**Re-Os geochronology of the Monterey Formation, Union Leroy  
51-18 well, Santa Maria Basin, California**

**A Thesis Presented to the  
Faculty of the Department of Earth and  
Atmospheric Sciences  
University of Houston**

**In Partial Fulfillment  
Of the requirements of the Degree  
Master of Science**

**By**

**Clint Barnette**

**August 2015**

## Abstract

The Os isotopic composition of marine Miocene strata records chronological variations in the world's oceans. These Os-isotope variations exhibit changes in global seawater geochemistry that result from tectonic, paleoclimate and extraterrestrial processes. The Os-isotopic record of seawater throughout the Miocene has studied elsewhere, but there are no  $^{187}\text{Re}$ - $^{187}\text{Os}$  isotope data available for the Monterey Formation, specifically during Serravallian time. The Serravallian Monterey has two predominant lithofacies of siliceous-shale and phosphatic-carbonate shale. In this study,  $^{187}\text{Re}$ - $^{187}\text{Os}$  isotope data, Rock-Eval and total organic carbon (TOC) data were obtained on samples from Serravallian Monterey Formation. The samples were acquired from core extracted from the Union Leroy 51-18 well in the Santa Maria Basin.

$^{187}\text{Re}$ - $^{187}\text{Os}$  geochronology of marine, organic-rich mud rocks from the Miocene Monterey Formation, Santa Maria Basin, California yields a scatterchron Model 3 age of  $11.5 \pm 1.5$  Ma (13% age uncertainty,  $2\sigma$ ,  $n=28$ , mean square of weighted deviates [MSWD]=112), which agrees within uncertainty with the expected age of this formation based on regional correlation of biostratigraphy and bentonite age data, and is the first direct, absolute  $^{187}\text{Re}$ - $^{187}\text{Os}$  age for the Monterey Fm. in the Santa Maria Basin. The initial  $^{187}\text{Os}/^{188}\text{Os}$  ( $^{187}\text{Os}/^{188}\text{Os}$ )<sub>i</sub> =  $0.78 \pm 0.04$  obtained by isochron regression represents the seawater  $^{187}\text{Os}/^{188}\text{Os}$  during the Serravallian for the Santa Maria Basin, and is substantially less radiogenic than the  $^{187}\text{Os}/^{188}\text{Os}$  of modern-day seawater ( $\sim 1.06$ ). Both radiogenic Os from continental weathering ( $^{187}\text{Os}/^{188}\text{Os} = \sim 1.4$ ) and non-radiogenic Os from mantle and extraterrestrial sources ( $^{187}\text{Os}/^{188}\text{Os} = \sim 0.13$ ) cause variations in the  $^{187}\text{Os}/^{188}\text{Os}$  of seawater that are recorded with marine ORM (organic-rich mud rock) deposition. Small-scale changes between the siliceous-shale and phosphatic-carbonate shale just based on calculated ( $^{187}\text{Os}/^{188}\text{Os}$ )<sub>i</sub> and stratigraphic depth were not resolvable, but incorporating

TOC and rock-eval data with the  $^{187}\text{Re}$ - $^{187}\text{Os}$  isotope data helps better understand depositional environment differences between the two lithofacies. Comparing the slopes of TOC plotted against Os abundances (ppt) suggests that the phosphatic-carbonate shale was deposited during a period of relatively higher sea level in a less restricted basin than the conditions of the siliceous-shale, which reinforces previously suggested depositional environments (Mackinnon, 1989).

## Table of Contents

1.1. Introduction	1
1.2. Geologic Setting	6
1.3. Previous Work	12
1.4. Sampling and Analytical Methods	14
1.4.1. $^{187}\text{Re}$ - $^{187}\text{Os}$ Isotope Geochemistry	14
1.4.2. Organic Characterization (TOC and Rock-Eval Pyrolysis)	17
1.5. Results	18
1.5.1. $^{187}\text{Re}$ - $^{187}\text{Os}$ Isotope Geochemistry	18
1.5.2. Organic Characterization (TOC and Rock-Eval Pyrolysis)	23
1.6. Discussion	27
1.6.1. $^{187}\text{Re}$ - $^{187}\text{Os}$ Geochronology	27
1.6.2. Comparison to established age	28
1.6.3. Re and Os Uptake and Fractionation in Restricted Basinal Systems	29
1.6.4. TOC with depositional conditions	36
1.6.5. Effects of Organic Matter Type	40
1.6.6. Os isotope implications of $(^{187}\text{Os}/^{188}\text{Os})_i$ at 11.5 Ma	48
1.7. Conclusion	51

## List of Figures

<b>Figure 1</b>	<b>Location and stratigraphic column of the Union Leroy 51-18 well</b>	<b>7</b>
<b>Figure 2</b>	<b>Stratigraphic column of the Santa Maria Basin</b>	<b>8</b>
<b>Figure 3</b>	<b>Union Leroy 51-18 Facies</b>	<b>10</b>
<b>Figure 4</b>	<b>Scatterchrons of the Sample Set</b>	<b>22</b>
<b>Figure 5</b>	<b>Total Organic Carbon plotted against depth</b>	<b>23</b>
<b>Figure 6</b>	<b>Modified van Krevelen Diagram</b>	<b>26</b>
<b>Figure 7</b>	<b><math>(^{187}\text{Os}/^{188}\text{Os})_i</math> plotted against depth</b>	<b>28</b>
<b>Figure 8</b>	<b>TOC/Mo data from MacArthur 2008</b>	<b>32</b>
<b>Figure 9A</b>	<b>TOC versus Re abundances of this study &amp; other studies</b>	<b>34</b>
<b>Figure 9B</b>	<b>TOC versus Os abundances of this study &amp; other studies</b>	<b>35</b>
<b>Figure 10</b>	<b>TOC versus Re and Os abundances of this study</b>	<b>38</b>
<b>Figure 11</b>	<b>TOC versus Re and Os abundances without outlier data</b>	<b>39</b>
<b>Figure 12</b>	<b>Modified van Krevelen Diagram with selected data points from Curiale and Odermatt (1989) and this study</b>	<b>41</b>
<b>Figure 13</b>	<b>Hydrogen Index plotted against Re and Os abundances</b>	<b>43</b>
<b>Figure 14</b>	<b>Hydrogen Index plotted against Re and Os abundances without outlier data</b>	<b>44</b>
<b>Figure 15</b>	<b>Oxygen Index plotted against Re and Os abundances</b>	<b>46</b>
<b>Figure 16</b>	<b>Oxygen Index plotted against Re and Os abundances without outlier data</b>	<b>47</b>
<b>Figure 17</b>	<b><math>(^{187}\text{Os}/^{188}\text{Os})_i</math> record from 20 Ma to 5 Ma</b>	<b>50</b>
<b>Table 1</b>	<b><math>^{187}\text{Re}</math>-<math>^{187}\text{Os}</math> data of the 28 samples from this study</b>	<b>20</b>
<b>Table 2</b>	<b>Rock-Eval and Pyrolysis Data</b>	<b>24</b>

## 1.1. Introduction

The  $^{187}\text{Re}$ - $^{187}\text{Os}$  isotope system has become an important tool in the geosciences. Rhenium and Osmium preferentially partition into metallic and sulphide phases in solid-melt systems as highly siderophile and chalcophile elements (Hart and Ravizza, 1996; Burton et al., 1999). This distinct behavior of Re and Os relative to other well-established lithophile isotope systems such as the Rb-Sr, Sm-Nd and U-Th-Pb isotope systems has resulted in new insights on a wide range of geological, geochemical and cosmochemical problems. For example, the  $^{187}\text{Re}$ - $^{187}\text{Os}$  isotope system has been crucial for understanding sulfide ore genesis (e.g., Hirt et al., 1963; Luck and Allegre, 1982 and others), determining crystallization ages of solar system materials (Luck et al., 1980; Luck and Allegre, 1983; Brandon et al., 2000), and better understanding crustal and mantle evolution (Herzberg, 1993; Walker, 1994).

The difference in compatibility between Re and Os is what makes the  $^{187}\text{Re}$ - $^{187}\text{Os}$  isotope system useful for geochemistry. Rhenium behaves incompatible and Os behaves moderately compatible during mantle melting (Walker et al., 1989). Because of these differences, the majority of Re is partitioned into the melt, and ultimately enriched in the earth's crust as mantle-derived melts ascend into the crust. In contrast, Os remains behind in mantle phases and is depleted in the Earth's crust relative to Re. The result of this is low Re/Os ratios in the mantle, and higher Re/Os ratios in the crust. This relative enrichment of Re in the crust coupled with the isotopic decay of  $^{187}\text{Re}$  to  $^{187}\text{Os}$  leads to crustal enrichment in  $^{187}\text{Os}$  with time. This process means that older crustal rocks, on average, will have much higher  $^{187}\text{Os}/^{188}\text{Os}$  ratios than younger crustal rocks, both of which have  $^{187}\text{Os}/^{188}\text{Os}$  ratios higher than the mantle, where latter has an average accepted present-day  $^{187}\text{Os}/^{188}\text{Os}$  ratio of 0.127 (Cohen, 2004).

In addition to Re and Os being chalcophile and highly siderophile they are both organophilic under anoxic, reducing conditions and therefore have an affinity for organic

complexes (Crusius et al., 1996). This affinity for organic complexes leads to relatively high abundances of Re and Os in organic-rich mud rocks (ORM). Hence the  $^{187}\text{Re}$ - $^{187}\text{Os}$  isotope system is ideal to evaluate conditions that enable ORM deposition including those found within lacustrine and marine basins. These elements immediately become sequestered in the water column, but it has not been determined if the elements are sequestered through an adsorption process or complexed within organic matter (Miller, 2004). The  $^{187}\text{Os}/^{188}\text{Os}$  signature of seawater is recorded in ORM at the time of deposition, and provides a record of seawater changes over time, influenced by mechanisms such as weathering, climate and tectonics (Esser and Turekian, 1988; Peucker-Ehrenbrink et al., 1995).

Recent advances in analytical techniques have created new opportunities for the precise, direct dating of ORM using the  $^{187}\text{Re}$ - $^{187}\text{Os}$  isotope chronometer (e.g., Shirey and Walker, 1995, Volkening et al., 1991, Creaser and Selby, 2002, Tripathy et al., 2014). Rhenium and Os are typically present in ORM in parts-per-billion (ppb) and parts-per-trillion (ppt) quantities. These sedimentary rocks are enriched in Re and Os by orders of magnitude when compared to other crustal lithologies that are typically in the 10s to 100s of ppt in abundance for these elements (Esser and Turekian, 1993; Horan et al., 1994). Precise measurement of  $^{187}\text{Re}$ - $^{187}\text{Os}$  isotopes and concentrations can be performed with less-than-1-gram quantities of bulk rock ORM samples (Creaser et al., 2002).  $^{187}\text{Re}$  decays to  $^{187}\text{Os}$  with a half-life of 41.6 billion years (Ga), and it is possible to use this chronometer to determine an age of deposition of ORM (Kendall et al., 2004) provided that (1) sufficient fractionation between Re and Os occurs within the suite of samples studied to produce a wide range in the Re/Os ratios of different rock samples, (2) all samples within the suite possessed the same initial  $^{187}\text{Os}/^{188}\text{Os}$  ratio at the time of deposition, and (3) there was no post-depositional mobilization of Re or Os (i.e., the system remained closed).

The  $^{187}\text{Re}$ - $^{187}\text{Os}$  isotope chronometer was first applied to ORM by Ravizza and Turekian

(1989) on the Bakken Shale in the Williston Basin (USA). This study obtained an age of  $354 \pm 49.2$  Ma ( $\pm 13.8\%$ ,  $2 \sigma$ ) using the now outdated nickel sulphide fire assay technique. The nickel sulphide fire assay technique produced results which are in agreement with the accepted age of the Bakken of  $\sim 360$  Ma (LeFever et al., 1991). Following Ravizza and Turekian (1989), Cohen et al. (1999) pioneered the use of high-temperature Carius-tube digestion using inverse *aqua-regia*, comprising a 1:2 mix of HCl to HNO<sub>3</sub>, to dissolve ORM. This Carius-tube method provided a means for adequate sample dissolution and thorough sample-spike equilibration (Shirey and Walker, 1995).

Sample selection and chemical extraction techniques have advanced substantially in the last decade, resulting in shale <sup>187</sup>Re-<sup>187</sup>Os isochrons with better precision. The largest step forward has been the implementation of Jones Reagent (Cr<sup>VI</sup>O<sub>3</sub> in H<sub>2</sub>SO<sub>4</sub>) as a digestion reagent (Selby and Creaser, 2003). Several studies have shown that dissolving ORM samples using inverse *aqua-regia* accesses both the hydrogenous (sea-water derived), and the non-hydrogenous, detrital material component of bulk rock ORM. However, these <sup>187</sup>Re-<sup>187</sup>Os studies are only concerned with the hydrogenous component (<sup>187</sup>Re-<sup>187</sup>Os) complexed with sulphides and organic carbon), and any non-hydrogenous Re and Os dissolved during digestion result in isochrons with larger uncertainties. This is because detrital, non-hydrogenous material in a single rock can be derived from multiple sources and thus can have widely varying Re and Os concentrations and <sup>187</sup>Os/<sup>188</sup>Os ratios with no age correlation with hydrogenous Re and Os. Hence accessing Re and Os in detrital material in ORM will likely result in greater scatter in the <sup>187</sup>Re-<sup>187</sup>Os isotope systematics and consequent detrimental effects to obtaining precise isochron ages of a related suite of ORM. Selby and Creaser (2003) developed the application of the Jones Reagent dissolution, and reported an age of  $363.4 \pm 5.6$  Ma ( $\pm 1.5\%$ ,  $2 \sigma$ ) for the Exshaw (black shale) Formation, Canada. The Exshaw sample, when digested with inverse *aqua-regia* accesses detrital

Re and Os, resulted in a less accurate age of  $358 \pm 10$  Ma ( $\pm 2.8\%$ ,  $2 \sigma$ ). From these results, Selby and Creaser (2003) concluded that the Jones Reagent, an organic oxidizer, only accesses the hydrogenous Re and Os of ORM. In their study, the Jones Reagent produced an uncertainty significantly lower than any previous method. Currently, with careful sample selection, preparation, and digestion using Jones Reagent, uncertainties of better than  $\pm 1\%$  ( $2 \sigma$ ) are achievable.

Changes in seawater chemistry are preserved in the rock record and predominantly interpreted using Sr, C and O isotopes. Osmium has joined these elements in becoming a useful isotopic tracer to understand seawater evolution in varying time intervals. The ORM Os isotope composition of a certain stratigraphic interval reflects the  $^{187}\text{Os}/^{188}\text{Os}$  composition of seawater at time of sediment deposition. Seawater evolution studies utilizing  $^{87}\text{Sr}/^{86}\text{Sr}$  isotopes are impeded by a lower-resolution residence time of 1-4 million years that results in longer averaged time variation of  $^{87}\text{Sr}/^{86}\text{Sr}$  isotopic values relative to  $^{187}\text{Os}/^{188}\text{Os}$ . By comparison, the residence time of Os is  $\sim 10$ -50 kyr (Peucker-Ehrenbrink and Ravizza, 2000). Hence, the shorter residence time of Os enables high-frequency seawater isotopic changes (such as glacial cycles) to be resolvable that are not resolvable when employing the  $^{87}\text{Sr}/^{86}\text{Sr}$  isotopic method.

Two primary inputs influence the  $^{187}\text{Os}/^{188}\text{Os}$  of seawater. Relatively non-radiogenic Os is contributed to seawater from the mantle by seafloor spreading processes (mid-ocean ridge basaltic magmatism and hydrothermal alteration of oceanic crust), and the emplacement of mantle plume-related Large Igneous Provinces in the ocean (eg., Ontong Java, Kerguelen, Caribbean). Non-radiogenic Os is also contributed from meteorite influx (Puecker-Ehrenbrink and Ravizza, 2000). Both mantle-derived material and meteorites have low Re/Os ratios compared to the Earth's crust and consequent time integrated relative low  $^{187}\text{Os}/^{188}\text{Os}$  ratios. Radiogenic Os is contributed by continental river runoff that carries weathered upper-continental

crust to seawater (Esser and Turekian, 1993). This is a result of the aforementioned high Re/Os ratios of the crust relative to the mantle with consequent time integrated relative high  $^{187}\text{Os}/^{188}\text{Os}$  ratios, respectively. The balance of these contributions to global seawater has varied substantially over time, and measuring the  $^{187}\text{Os}/^{188}\text{Os}$  of different ORM enables the reconstruction of the  $^{187}\text{Os}/^{188}\text{Os}$  of seawater at time of deposition, and therefore seawater evolution. Studies such as Poirier and Hillaire-Marcel (2011) have successfully used  $^{187}\text{Os}/^{188}\text{Os}$  values over time to determine stratigraphic transitions of depositional environments and see how well these data fit into the established  $(^{187}\text{Os}/^{188}\text{Os})_i$  seawater curve.

The aforementioned short residence time of Os of <10,000 years means that  $^{187}\text{Os}/^{188}\text{Os}$  data for ORM can provide high-resolution data on the global climate and water cycle, and help understand on the regional and basinal depositional environment. Determining the ratios of  $^{187}\text{Re}/^{188}\text{Os}$  and present-day  $^{187}\text{Os}/^{188}\text{Os}$  enables one to calculate the  $(^{187}\text{Os}/^{188}\text{Os})_i$  of seawater at time of deposition of ORM. In restricted basins,  $(^{187}\text{Os}/^{188}\text{Os})_i$  stratigraphy can be helpful in determining stratigraphic and depositional transitions, especially when the basin has undergone restriction for unknown lengths of time.

One basin that has experienced various degrees of restriction for poorly understood lengths of time is the Santa Maria Basin, California. This study presents  $^{187}\text{Re}$ - $^{187}\text{Os}$  geochemical and geochronological data for subsurface samples of the thermally immature, organic-rich, Serravallian Monterey Formation. The goals of the study are to interpret the  $^{187}\text{Re}$ - $^{187}\text{Os}$  isotopic chemistry of seawater in the Santa Maria Basin during the Serravallian and to obtain an absolute age for the time of ORM deposition within the basin. This study provides an approximate age for the Serravallian Monterey Fm. In addition, the Re and Os behavior is examined by pairing these data with total organic carbon (TOC) and Rock-Eval data to better understand depositional conditions across a facies boundary within the Monterey Fm.

## **1.2. Geologic Setting**

This study focuses on the mid-Miocene Monterey Formation of the Union Leroy 51-18 well in the Santa Maria Basin in Southern California (Figure 1). The Monterey Formation was deposited in the Santa Maria Basin from 17.5 Ma until approximately 6 Ma, when a regional tectonic event isolated the basin and cut off deposition (Figure 2; Mackinnon, 1992). Changes in Pacific Ocean circulation and increased global cooling were the catalysts that initiated Monterey deposition along the California coast, enhancing oceanic upwelling and diatom productivity. Geologic and geochemical data suggest the Santa Maria Basin depositional environment during the Miocene was a sediment-starved dysaerobic to anoxic marine basin (Curiale and Odermatt, 1988).

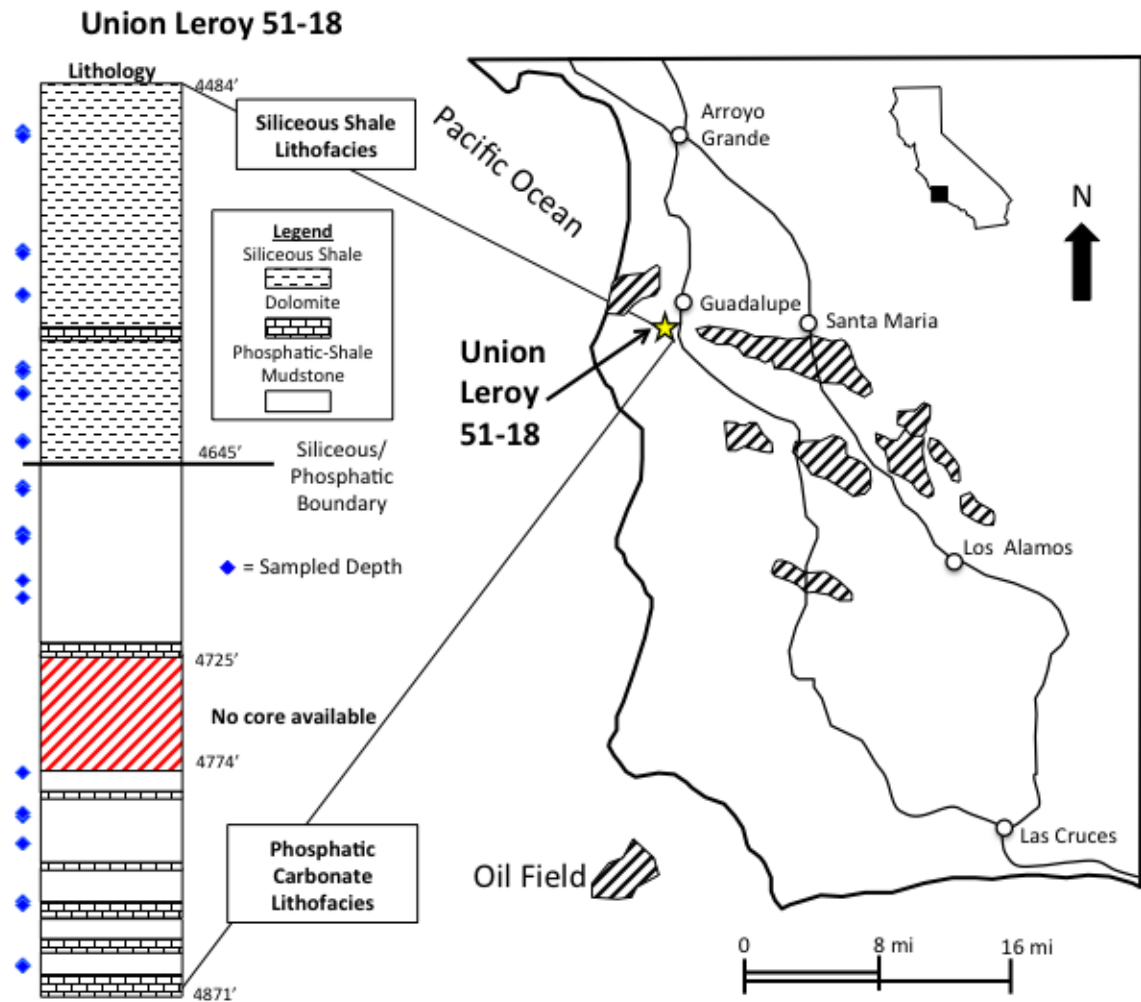


**Figure 1: Location and stratigraphic column of the Union Leroy 51-18 well in the Santa Maria Basin, map based on Curiale and Odermatt (1989) and stratigraphic column based on Odermatt and Curiale (1991).**

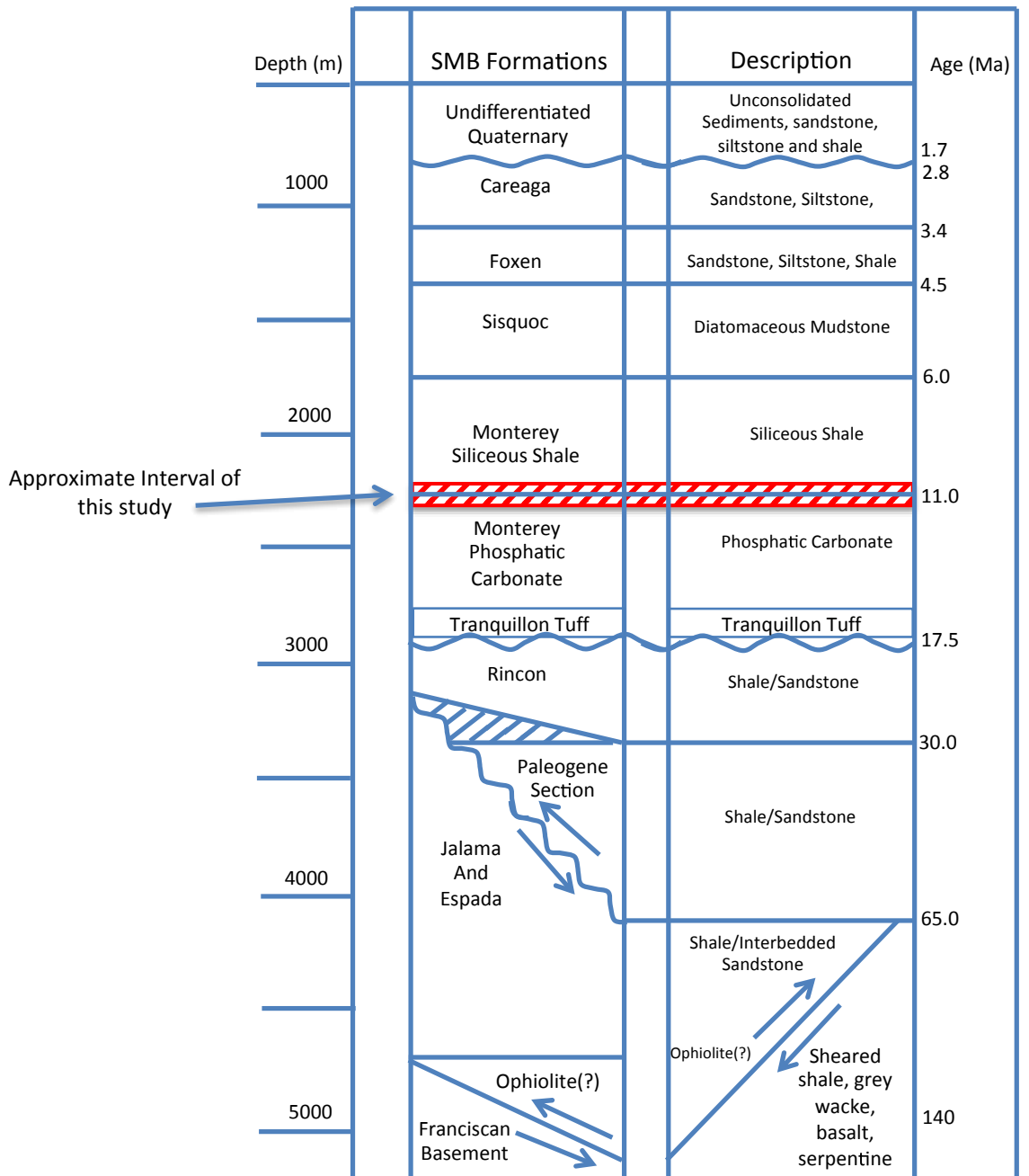


**Figure 2: An approximate stratigraphic column of the entire Santa Maria Basin. The middle shaded area represents this study’s interval of Monterey, and also highlights the Monterey facies boundary in context with the rest of the Santa Maria Basin (Modified after Nicholson, 1992)**

The Santa Maria Basin was part of a larger subduction-forearc basin system from Jurassic

to the Oligocene that spanned most of what is now southern California. In the late Oligocene-early Miocene, the California margin experienced rapid downdropping and development of deep marine coastal basins occurred (Mackinnon, 1992). Highly deformed and metamorphosed sedimentary rocks present within the stratigraphic successions indicate that the Santa Maria area in particular is where the majority of this subduction occurred (Isaacs, 1992). After 29 Ma, the Santa Maria tectonic system changed to a transform margin, resulting in formation of new marine basins and substantial extension and subsidence (Isaacs, 1992). The Transverse Ranges block rotated during this time period, creating a series of outer basins and a series of inner basins. The outer basins, including the Santa Maria Basin, were protected from terrigenous sediment influx whereas the inner basins became depositional centers. With little to no terrigenous influx, siliceous and calcareous sediment derived from the photic zone rapidly accumulated in the Santa Maria Basin until 6 Ma (Mackinnon, 1992). The active tectonic history of the Santa Maria Basin and surrounding area impacts the subsurface distribution of the Miocene section, and complicates geochemical evaluation.

The Monterey Formation is 2000 to 4500' thick, and has significant fracturing toward the edges of the Santa Maria Basin (Isaacs, 1992). The section of core utilized for this study is from the Union Leroy 51-18 well, and has two major lithofacies (Curiale and Odermatt, 1989). A siliceous-shale lithofacies overlies a phosphatic shale and carbonate lithofacies (Curiale and Odermatt, 1989) (Figure 2). Samples were taken from both facies fully representing the extent of core section. The phosphatic-shale-and-carbonate facies are referred to as the phosphatic-carbonate facies in the remainder of this paper.



**Figure 3. Pictures of the phosphatic-carbonate (left) and siliceous-shale (right) facies from the Union Leroy 51-18 core. The phosphatic-carbonate facies sample is at 4830' and sample M-25. The siliceous-shale facies is at 4574' and sample M-03. Note the bedding and coloration differences between the two. The core is 6 inches wide.**

The Phosphatic-carbonate facies is usually laminated, and contains greater than 50% calcite and dolomite thought to be deposited as a coccolith/foraminiferal diatom mud (Mackinnon, 1992). This facies was formed in a low-oxygen environment dominated by calcareous sedimentation (Schwalbach and Bohacs, 1992). The low-oxygen environment is interpreted to be

an oxygen-minimum zone in the bottom water column, reinforced by a lack of burrowing and presence of massive bedding. Oxygen-minimum zones are found in environments such as outer shelf, slope, basin floor, or deeply submerged banks, and enhance preservation of organic matter. The small-scale laminations of the phosphatic shale reflect seasonal changes in sediment supply (Schwalbach and Bohacs, 1992). The dark layers are detritus-rich, due to high rainfall and water runoff and are interpreted to be associated with winter depositional times. The lighter layers are concentrations of undiluted biogenic siliceous matter and are interpreted to be associated with the warmer temperatures of summer (Schwalbach and Bohacs, 1992). The phosphatic-carbonate facies also has 1-to-3-cm-thick altered ash/tuff layers in the lower part of the section. However it's unclear if the section of Union Leroy 51-18 core in this study has ash or tuff layers.

The siliceous-shale facies of the Monterey Fm. overlies the phosphatic-carbonate facies. This facies is predominantly comprised of biogenic silica, shell forming plants and animals, and diatoms (Schwalbach and Bohacs, 1992). The total production of biogenic silica is dictated by available nutrient supply, which is primarily influenced by upwelling zones, although volcanic ash is an additional source of Si and can produce blooms. Upwelling zones are caused by winds and ocean currents that displace surface water and bring nutrients to the surface (Schwalbach and Bohacs, 1992). Nutrients such as phosphorus and nitrogen, from the decay of biogenic organisms, are brought to the surface by upwelling waters. Upwelling zones can increase total productivity by an order of magnitude compared to areas lacking upwelling (Mackinnon, 1989). For the Monterey Fm. specifically, basin fractionation between the Atlantic and Pacific Oceans changed ocean current patterns, and resulted in increased silica-rich bottom water flow in the Pacific (Schwalbach and Bohacs, 1992). Oceanic upwelling along the California margin began in the early-mid Miocene as well, providing ideal conditions for biogenic-silica deposition (Schwalbach and Bohacs, 1992). Sea level decreased throughout the mid Miocene, making upwelling more

effective in circulating nutrients from the sea floor to the surface (Schwalbach and Bohacs, 1992). As in the phosphatic-carbonate facies, oxygen minimum zones preserved the organic matter in the siliceous-shale facies (Mackinnon, 1989).

Samples from both lithofacies were measured for  $^{187}\text{Re}$ - $^{187}\text{Os}$  isotopes. The samples targeted had visual signs of being enriched in total organic carbon (TOC). Curiale and Odermatt (1989) determined that this section of the Union Leroy 51-18 well is thermally immature (vitrinite reflectance=0.3-0.5%  $R_o$ ), and hence the  $^{187}\text{Re}$ - $^{187}\text{Os}$  isotope systematics within the samples have likely not experienced disturbance since lithification. The Monterey Formation contains bentonite (volcanic ash) beds throughout and it has been extensively studied using biostratigraphy, thus providing independent age constraints (Hornafius, 2009).

### **1.3. Previous Work**

The Union Leroy 51-18 is located within the area where the combined source-reservoir character of the Monterey is most pronounced, sampled from the core depths of 4484' to 4854' and annotated in Figure 1 (Curiale and Odermatt, 1989). This section of the Union Leroy 51-18 well has been the focus of two studies (e.g. Curiale and Odermatt, 1989, Curiale and Odermatt, 1991).

The first study, Curiale and Odermatt (1989), evaluated short-term biomarker variability in samples spanning the section using the TOC content, Rock-Eval pyrolytic yield, vitrinite reflectance, and the distribution of steranes, terpanes, and aromatics. They determined that the temperature variation across the entire core section is only 5° Celsius. This minor maturity difference in section means that the small-scale geochemical variations are more indicative of facies depositional environment and source rock quality, as opposed to reflecting maturity variations. The distribution of steranes, terpanes, and aromatics gradually changed over the

section, but there was a clear facies boundary based on the kerogen values between the phosphatic-carbonate shale and the siliceous-shale intervals, with the phosphatic-carbonate facies having higher kerogen contents and therefore possessing a higher source rock potential. High concentrations of aromatic steroids and 28,30 bisnorhopane were found in this study, which reflects a massive input of anaerobic biota (Curiale and Odermatt, 1989).

The second study, Odermatt and Curiale (1991), examined small-scale variations in organically bound Cr, Mo, Ni, and V, of the same section and compared them to the biomarker variations of the previous study. The cross-plots of kerogen versus bitumen for  $V/(V+Ni)$  and  $Mo/(Mo+Cr)$  all had correlations greater than 0.8, consistent with a genetic relationship between kerogen concentrates and extractable organic matter (EOM) in the Monterey. These same compositional relationships also delineate the facies differences between the siliceous-shale and the phosphatic-carbonate shale, as the data from each facies plot as distinctive groups. Odermatt and Curiale (1991) determined that V, Mo and Cr correlate with kerogen and EOM. There was, however, too much inorganic Ni present in the samples to significantly correlate between the kerogen and bitumen. As with the kerogen facies boundary discussed in the previous paragraph, there is a clear trend break between the facies for V, Mo, and Cr, highlighting another difference between the two lithologies and likely a function of differences in their depositional environments.

The Monterey Formation also contains a rich assortment of bentonite beds that can be used to provide age constraints for comparison with those obtained using the  $^{187}Re-^{187}Os$  isotope system. Hornafius (1994) established five chemically distinct Monterey ash bed zonations at Naples Beach (California). These zonations were used to correlate with other stratigraphic sections in Southern California. The zonations were based on the ash compositions using La, Sm, Yb, Nb, Th, Ti, and Zr. These elements are relatively immobile during the alteration of ashes to

tuffs or bentonites, and hence can be used for correlations between distinct units (Hornafius, 1994). The oldest ash, Zone 1t, is the Tranquillon tuff. Rubidium-strontium and  $^{40}\text{Ar}/^{39}\text{Ar}$  dating combined with biostratigraphy place the top of the Tranquillon tuff at 17.6-17.9 Ma (Hornafius, 1994). Zone 2 is a stratigraphically repeated interval that is soft-sediment deformed and has different thicknesses and layering characteristics. This interval is interpreted to comprise multiple air fall deposits from a single volcanic center (Hornafius, 1994). The best constraint on the age of Zone 2 is approximately 16.5-17.5 Ma (Hornafius, 1994). Zones 1o and 3 have overlapping ranges in ash bed age, with age ranges of 15.3-16.5 and 13.8-15.1 Ma, respectively. Zone 4 is defined by its own group of ash intervals, with an age range of 9.1-13.8 Ma (Hornafius, 1994). Zone 5 is another concurrent range zone, with only the base being confidently evaluated with an age of at least 11.3 Ma. The top of Zone 5 has diatoms (*D. hustedtii*-*D. lauta*) that have an age range of 8.4-8.9 Ma, but there wasn't a large enough quantity of *D. hustedtii*-*D. lauta* to accurately constrain the youngest age of Zone 5 (Hornafius, 1994). These 5 independently evaluated sequential zones of the Monterey reinforce the Monterey deposition age as ranging from 17.6-17.9 Ma to at least 8.4-8.9 Ma, and provide an approximate age framework for this study. Based on the results of this study, both the siliceous-shale and phosphatic-carbonate lie entirely within the ranges of Zone 4, and the base of Zone 5 could also lie within the age ranges of the siliceous-shale and phosphatic-carbonate. The boundary between siliceous-shale and phosphatic-carbonate facies has been identified to be at 11 Ma (Behl, 2012)

## **1.4. Sampling and Analytical Methods**

### **1.4.1. $^{187}\text{Re}$ - $^{187}\text{Os}$ Isotope Geochemistry**

The Monterey rock samples used in this study were taken from the Unocal-drilled Union Leroy 51-18 core which is currently curated at the Houston Branch of the Texas Bureau of

Economic Geology Core Repository. The core interval in this study is the same as that of Curiale and Odermatt (1989) and Odermatt and Curiale (1991), with all sampling from the Monterey Formation. Half-inch to 1-inch thick slices were first taken from the organic-rich parts of the core identified from the studies mentioned above. Samples were also taken from other non-organic-rich parts of the core to better represent the full interval and represent the contact between the phosphatic-carbonate and siliceous-shale lithofacies. Twenty-eight samples were taken from the core for analysis.

All outside surfaces of the core samples were sanded with silicon carbide to remove all surfaces that may have come in contact with metal coring equipment, and then cleaned with ethanol. The core samples were powdered using ceramic alumina grinding surfaces in a shatter box to obtain a homogenous, metal-free, fine-grained whole-rock powder. The sample powders were separated into individual aliquots representative of each core sample for bulk rock Re and Os concentrations, Os isotopic composition, and organic characterization.

Approximately 0.3 g of sample powder was weighed and combined with a known amount of  $^{185}\text{Re} + ^{190}\text{Os}$  spike and 8 mL of Jones Reagent ( $0.25\text{g Cr}^{\text{VI}}\text{O}_3 / 1 \text{ mL H}_2\text{SO}_4$ ) in a borosilicate glass Carius tube sealed and then digested for approximately 48 hrs at  $240^\circ\text{C}$ . As aforementioned, the Jones Reagent preferentially dissolves and oxidizes hydrogenous Re and Os, which results in more accurate and precise Os ages (Selby and Creaser, 2003). During digestion, organically bound Re and Os within bulk rock powders are mostly oxidized to  $\text{ReO}_3^-$  and  $\text{OsO}_4^-$  and equilibrated with the spike. Following digestion, the Carius tubes were frozen in a slurry of ethanol and dry ice, opened, thawed and Os was subsequently removed from the digested solution through solvent extraction using chloroform ( $\text{CHCl}_3$ ) (Selby and Creaser, 2003). Chloroform effectively extracts  $\text{OsO}_4^-$  from oxidized solutions such as Jones Reagent. After solvent extraction, Os was back-extracted from the  $\text{CHCl}_3$  into  $\text{HBr}$  in order to reduce Os bonded in the

oxidized  $\text{OsO}_4^-$  into a less volatile form of  $\text{OsBr}_6^{2-}$ . This inhibited Os evaporation during dry down. The  $\text{HBr-OsBr}_6^{2-}$  solution was dried to an Os salt and purified by micro-distillation in an inverted conical Teflon vial (Birck et al., 1997). During micro-distillation, Jones Reagent was used to oxidize the Os in the dried salt, which became volatile. The volatile Os was trapped and reduced in a drop of  $\text{HBr}$  at the apex of the inverted conical vial. This procedure eliminated any contamination by other elements that may have been removed from the sample solution during solvent extraction. The remaining digested solution of the Carius tube (post Os-removal) was reduced from  $\text{Cr}^{\text{VI}}$  to  $\text{Cr}^{\text{III}}$  using a combination of Milli-Q bubbled with  $\text{SO}_2$  gas, and Re was subsequently removed via anion column chromatography. The output of the first Re column was further purified by passing through a second anion column. The isolated Re and Os was then loaded onto ultra-pure (>99.9%) nickel (Ni) and platinum (Pt) filaments, respectively, and coated with activator solutions of  $\text{Ba}(\text{NO}_3)^{2-}$  and  $\text{Ba}(\text{OH})^{2-}$ , respectively, to lower the ionization energy during heating in the mass spectrometer. The samples were analyzed using negative-thermal-ionization mass spectrometry (NTIMS) on a TRITON Plus TIMS at the University of Houston. Analytical conditions for NTIMS analyses mirror those outlined by previous researchers (e.g. Volkening et al., 1991; Creaser et al., 1991; Creaser and Selby, 2003).

Isotopic ratios measured from NTIMS analysis were spike- and mass fractionation-corrected. Procedural uncertainties were calculated through dissemination of blank isotopic abundance and composition, spike abundance, and reproducibility of the standard filament's Re and Os isotopic values. Procedural Re blanks for this study were 1.142 ppb, 0.288 ppb, and 0.294 ppb, respectively, for an average of 0.575 ppb. The first blank of 1.142 is significantly high compared to the target blank of 0.2 ppb Re, implying additional Re contamination somewhere in the geochemical process. Once the high blank was discovered, acids were re-made and additional protocols were taken to ensure it didn't happen again. The blanks of 0.288 and 0.294 ppb are

acceptable. The samples in this study are so young however, that the high Re blank value of 1.142 did not affect age or  $(^{187}\text{Os}/^{188}\text{Os})_i$  calculations. Procedural Os blanks for this study were 2.131 ppt, 0.219 ppt, and 0.438 ppt. As in the case for the aforementioned Re blanks, the first Os blank is significantly high. However, having the high Os blank from the same chemistry round as the Re blank reinforces that it was a lab contamination that caused the issue, as the last two Os blanks for 0.219 and 0.438 ppt were consistent with those obtained by others performing Re-Os isotope chemistry studies on ORM in the lab during the same time interval.

Rhenium and Os standards were repeatedly measured throughout NTIMS analysis. The Re standard yielded an average  $^{185}\text{Re}/^{187}\text{Re}$  ratio of  $0.59387 \pm 0.00125$  ( $2\sigma$ ) from 1.5 ng loads using standard faraday collection. Gramlich et al. (1973) established the Re standard value of  $0.59738 \pm 0.00390$  which is within error of the Re standard of this study, and used in reducing data and correcting  $^{185}\text{Re}/^{187}\text{Re}$  ratios. The average for the University of Maryland Os standard (Brandon et al., 1999) during the analytical campaign had a  $^{187}\text{Os}/^{188}\text{Os}$  ratio of  $0.11385 \pm 0.00026$  ( $2\sigma$ ,  $n=18$ ) for 500 pg loads, and this study's  $^{187}\text{Os}/^{188}\text{Os}$  average ratio was  $0.11405 \pm 0.00012$ , which is within uncertainty of that reported by Brandon et al. (1999). The  $(^{187}\text{Os}/^{188}\text{Os})_i$  and  $^{187}\text{Re}$ - $^{187}\text{Os}$  isotope age are calculated using Isoplot v. 3.75 (Ludwig, 2012).

#### **1.4.2. Organic Characterization (TOC and Rock-Eval Pyrolysis)**

Total organic carbon (TOC) content was calculated by the dry combustion of an aliquot of the powdered sample using a Leco CS340 Carbon Analyzer at the University of Houston Center for Petroleum Geochemistry, Houston, Texas. Samples were first separated into respective porous crucibles and pretreated with 2% HCl acid to dissolve any carbonate-associated carbon. The demineralized samples were then dried in a low-heat oven overnight. The dried crucible was then placed in the Leco CS340 Carbon Analyzer, and heated to  $1,350^\circ\text{C}$  in an oxygen atmosphere. The

oxidized carbon from this reaction forms CO<sub>2</sub>, which is carried through various scrubbers to remove impurities and residual moisture, and then measured by an infrared detector and converted to carbon as a weight percent (TOC).

Rock-Eval pyrolysis to determine organic matter type and maturity was completed using a Vinci Rock Eval II + Pyrolysis-Assay Analyzer at the University of Houston Center for Petroleum Geochemistry, Houston, Texas. Powdered samples are loaded into a turret with the Vinci programmed to heat each sample to approximately 300°C for three minutes to volatilize the bitumen within the sample. Bitumen, also known as free hydrocarbons already naturally generated within the sample, are reported in terms of mg of hydrocarbons per gram of TOC (mgHC/gTOC) and called S<sub>1</sub>. Once the bitumen is volatilized and evaluated, the temperature ramps from 300°C to 550°C, a hot enough temperature to volatilize kerogen, which is then evaluated and recorded as mgHC/gTOC and termed S<sub>2</sub>. After the free hydrocarbons have been removed, the temperature of maximum hydrocarbon formation is evaluated, and termed T<sub>max</sub>. T<sub>max</sub> is dependent upon the organic matter type and thermal maturity present in the sample. The final component measured during rock-eval pyrolysis is S<sub>3</sub>, an indication of the quantity of oxygen in kerogen, which is ultimately dependent upon organic matter type. S<sub>3</sub> is the term for CO<sub>2</sub> that is created during the thermal cracking of heavy carbon compounds and measured as mgCO<sub>2</sub>/gTOC.

## **1.5. Results**

### **1.5.1. <sup>187</sup>Re-<sup>187</sup>Os Isotope Geochemistry**

The <sup>187</sup>Re/<sup>188</sup>Os, <sup>187</sup>Os/<sup>188</sup>Os and Re and Os abundances are shown in Table 1. Compared to continental crust averages of ~1 ppb Re and 30-50 ppt Os (Esser and Turekian, 1993), all samples are enriched in Re (13-269 ppb) and almost all are enriched in Os (44-1332 ppt). There is one outlier sample (M-17) that's not enriched in Os with just 44 ppt. Besides this one low Os

value, the next lowest Os is 124 ppt, which is enriched related to modern day continental crust. These enriched Re and Os abundances are typical for ORM (eg., Ravizza and Turekian, 1989; Selby and Creaser, 2003; Rooney et al., 2010). The  $^{187}\text{Re}/^{188}\text{Os}$  values range from 634 to 2164 and positively correlate with  $^{187}\text{Os}/^{188}\text{Os}$  ratios of 0.88 to 1.18.

Sample	Depth	$^{187}\text{Re}/^{188}\text{Os}$	$^{187}\text{Os}/^{188}\text{Os}$	$^{187}\text{Os}/^{188}\text{Os}$	Re(ppb)	Os(ppt)	$\pm$	$(^{187}\text{Os}/^{188}\text{Os})$	$\pm$	TOC	Sulfur	Facies Designation
M-01	4504.0	1440.22	1.06	0.01	130.16	488.31	1.68	0.779	2.55	12.4	2.61	Siliceous Shale
M-16	4505.5	1723.93	1.10	0.00	52.35	164.87	0.69	0.767	0.54	4.8	0.95	Siliceous Shale
M-28	4506.5	1468.72	1.03	0.00	186.71	685.00	2.41	0.751	1.75	17.0	4.03	Siliceous Shale
M-02	4554.0	2034.31	1.16	0.01	256.11	688.11	3.28	0.765	3.15	18.3	4.02	Siliceous Shale
M-02-A	4554.0	2043.25	1.16	0.00	266.28	712.79	3.41	0.769	1.87	19.4	4.21	Siliceous Shale
M-02-B	4554.0	2122.68	1.17	0.00	268.85	693.27	3.44	0.760	1.79	18.6	4.13	Siliceous Shale
M-02-C	4554.0	2164.15	1.18	0.00	268.70	680.11	3.45	0.759	1.82	17.9	3.96	Siliceous Shale
M-02-D	4554.0	2104.63	1.17	0.00	255.89	665.49	3.38	0.764	1.72	18.6	4.10	Siliceous Shale
M-02-E	4554.0	2099.82	1.15	0.00	267.62	696.19	3.43	0.747	1.80	18.0	3.89	Siliceous Shale
M-17	4555.8	1611.99	1.11	0.01	13.01	43.88	0.18	0.803	0.27	16.6	0.74	Siliceous Shale
M-03	4574.0	1792.85	1.13	0.01	130.72	397.49	1.68	0.789	2.57	9.9	2.28	Siliceous Shale
M-04	4604.0	1741.70	1.18	0.01	146.31	460.14	1.88	0.840	2.50	10.5	2.05	Siliceous Shale
M-05	4614.0	1441.49	1.14	0.01	191.05	722.76	2.45	0.859	3.01	16.5	3.44	Siliceous Shale
M-06	4634.0	1438.00	1.04	0.01	205.85	771.65	2.64	0.760	3.68	16.1	3.50	Siliceous Shale
M-20	4634.8	1301.65	1.10	0.00	134.07	559.16	1.72	0.847	1.52	13.0	2.57	Siliceous Shale
M-07	4654.0	1457.52	1.11	0.02	58.71	218.86	0.76	0.825	2.07	8.7	1.53	Phosphatic Carbonate
M-07-Redb	4654.0	1550.10	1.08	0.00	65.17	227.85	0.84	0.784	0.67	8.7	1.53	Phosphatic Carbonate
M-08	4674.0	633.81	0.91	0.00	113.44	950.04	1.46	0.783	3.44	11.9	3.50	Phosphatic Carbonate
M-22	4676.0	677.51	0.91	0.00	161.56	1266.36	2.07	0.779	2.87	18.3	4.64	Phosphatic Carbonate
M-09	4693.0	763.92	0.89	0.00	159.93	1109.32	2.06	0.744	3.62	14.2	4.17	Phosphatic Carbonate
M-10	4700.3	786.51	0.92	0.00	197.09	1332.29	2.53	0.768	4.07	19.3	5.38	Phosphatic Carbonate
M-11	4774.0	892.62	0.95	0.01	121.50	726.70	1.56	0.783	3.09	10.6	2.19	Phosphatic Carbonate
M-23	4791.0	909.88	0.95	0.00	116.15	681.24	1.49	0.775	1.66	8.0	2.44	Phosphatic Carbonate
M-12	4793.0	722.02	0.93	0.01	45.19	333.08	0.59	0.789	2.30	5.5	1.49	Phosphatic Carbonate
M-13	4804.0	1016.27	1.00	0.00	215.62	1138.61	2.76	0.803	3.94	17.4	4.12	Phosphatic Carbonate
M-14	4828.8	736.57	0.88	0.00	116.80	839.00	1.51	0.736	3.22	8.7	3.31	Phosphatic Carbonate
M-25	4830.0	1006.45	0.99	0.00	157.49	838.85	2.02	0.795	2.04	12.8	3.30	Phosphatic Carbonate
M-15	4854.8	1003.62	0.91	0.03	23.48	124.21	0.31	0.713	1.77	1.7	0.82	Phosphatic Carbonate

Table 1:  $^{187}\text{Re}$ - $^{187}\text{Os}$  data of the 28 samples from this study

Rhenium and Os abundances and the  $^{187}\text{Re}/^{188}\text{Os}$  in the siliceous-shale facies range from 13-269 ppb, 44-772 ppt, and 1302-2164, respectively. By comparison, the phosphatic-carbonate facies samples have Re and Os abundances ranging from 23-216 and 124-1332 with a  $^{187}\text{Re}/^{188}\text{Os}$  ratio of 634-1550. The siliceous-shale facies has a higher average Re abundance (185 ppb) and average  $^{187}\text{Re}/^{188}\text{Os}$  ratio (1769) and the phosphatic-carbonate shale has a higher average Os abundance (753 ppt).

Linear regression of all 28 samples from this study provides a scatterchron age of  $11.5 \pm 1.5$  Ma (13% age uncertainty,  $2\sigma$ ,  $n=28$ ,  $\text{MSWD}=112$ ), Figure 3. This scatterchron yields an  $(^{187}\text{Os}/^{188}\text{Os})_i$  of  $0.779 \pm 0.037$ , a 4.74% uncertainty. In an attempt to reduce the age uncertainty, samples from the top 50 feet of the siliceous-shale facies were used to determine the age. This resulted in an age of  $11.1 \pm 1.7$  Ma (15.3% age uncertainty,  $2\sigma$ ,  $n=9$ ,  $\text{MSWD} = 9.9$ ), and an  $(^{187}\text{Os}/^{188}\text{Os})_i$  of  $0.777 \pm 0.056$ , a 7.21% uncertainty. Out of these two scatterchrons, the pooled isochron with all samples from this study best resolves the age and  $(^{187}\text{Os}/^{188}\text{Os})_i$  of the Serravallian Monterey Shale.

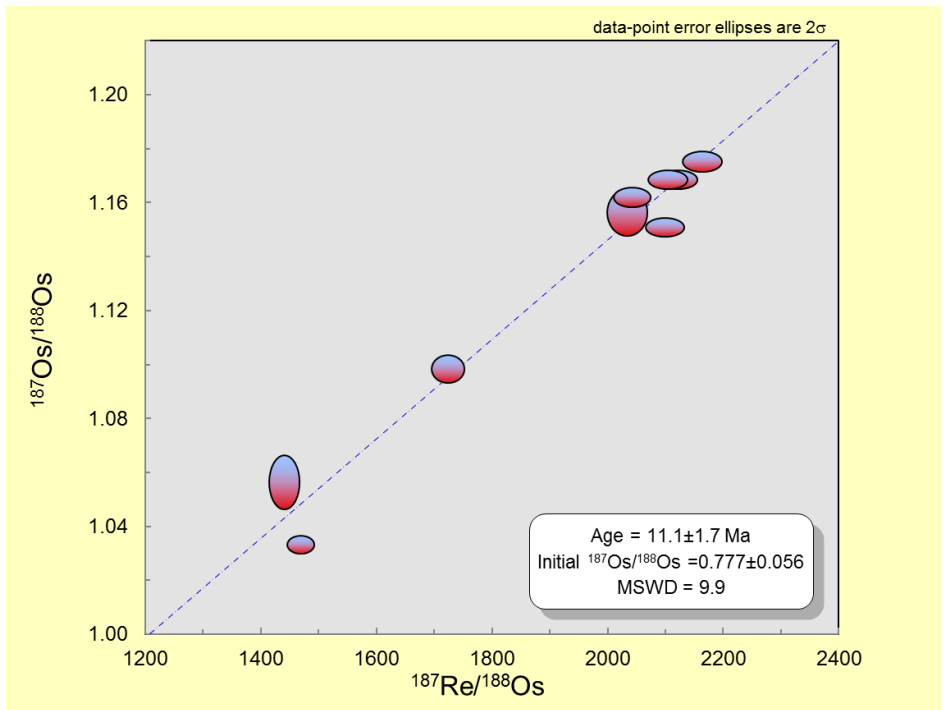
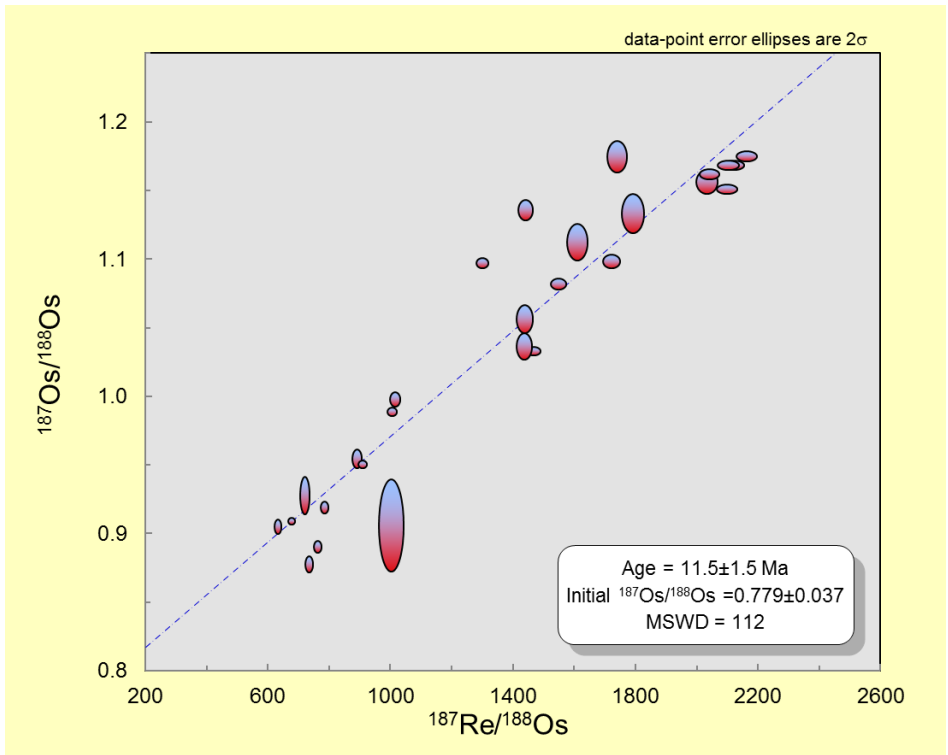


**Figure 4: Scatterchrons of the entire sample set (top) and the top 50 feet of the study section (bottom).**

### 1.5.2. Organic Characterization (TOC and Rock-Eval Pyrolysis)

The TOC values for the Monterey samples measured in this study range from 1.65 to 19.4 wt% with an average of 13.3 wt% for all samples from both facies. There is a slight trend to lower TOC as depth increases (Figure 4, Table 2). On a facies basis, the siliceous-shale has TOC values ranging from 4.8 to 19.4 wt% with an average of 15.2 wt%. The phosphatic-carbonate facies has TOC values ranging from 1.65 to 19.3 wt%, with an average of 11.2 wt%.

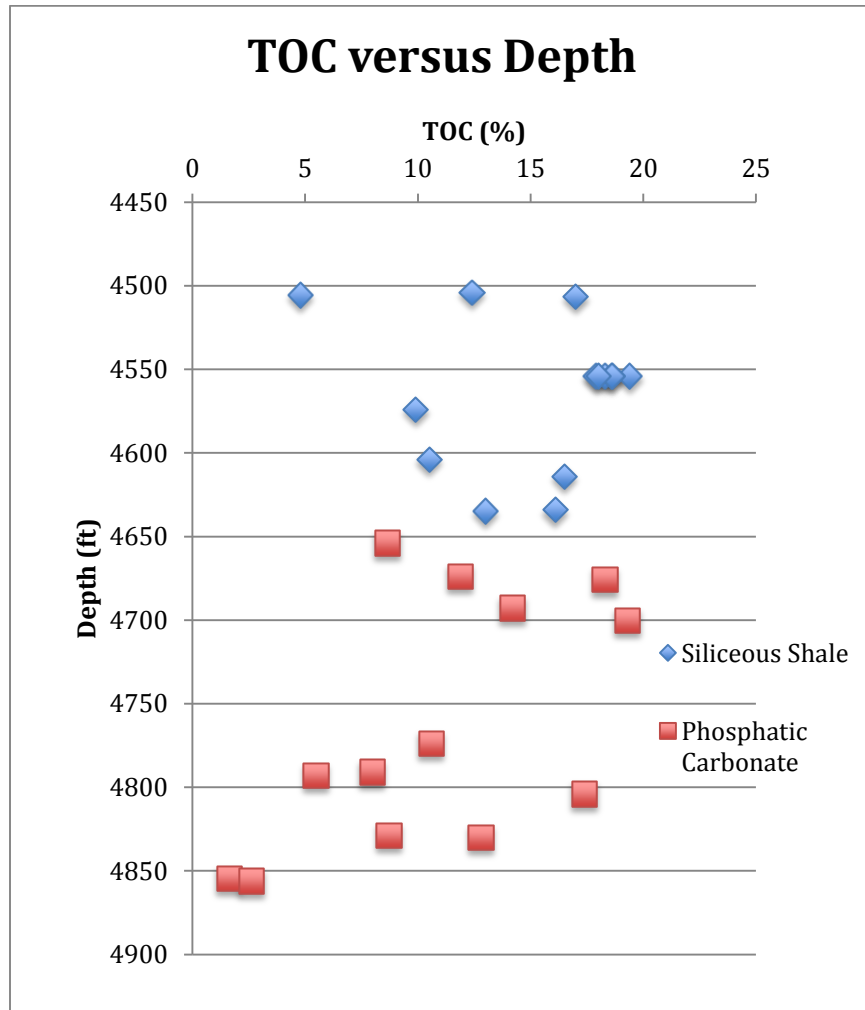


**Figure 5: Total organic carbon plotted against depth. The siliceous-shale facies has a higher average TOC than the phosphatic-carbonate.**

Sample		SOURCE QUALITY							THERMAL MATURITY		
Sample	Depth	Total Organic Carbon	Free Hydrocarbons	Generatable Hydrocarbons	Total Hydrocarbon Generation Potential	Hydrogen Enrichment Index	Generatable Carbon Dioxide	Oxygen Enrichment Index	Transformation Ratio	Temp. of Peak S <sub>2</sub>	
		TOC (%)	S <sub>1</sub> (mg HC/gm rk)	S <sub>2</sub> (mg HC/gm rk)	S <sub>1</sub> +S <sub>2</sub> (mg HC/gm rk)	HI (mg HC/gm TOC)	S <sub>3</sub> (mg CO <sub>2</sub> /gm rk)	OI (mg CO <sub>2</sub> /gm TOC)	"PI" (S <sub>1</sub> /S <sub>1</sub> +S <sub>2</sub> )		
M-01	4504	12.4	3.17	64.02	67.19	516	2.06	17	0.05	393	
M-16	4505.5	4.8	2.92	23.84	26.76	497	0.78	16	0.11	398	
M-28	4506.5	17	5.36	95.5	100.86	562	2.49	15	0.05	391	
M-02	4554	18.3	5.56	112.65	118.21	616	1.94	11	0.05	396	
M-02-A	4554	19.4	5.56	122.74	128.30	633	1.71	9	0.04	397	
M-02-B	4554	18.6	5.46	118.92	124.38	639	1.67	9	0.04	395	
M-02-C	4554	17.9	5.31	111.47	116.78	623	1.78	10	0.05	395	
M-02-D	4554	18.6	5.21	117.33	122.54	631	1.76	9	0.04	395	
M-02-E	4554	18	5.04	110.2	115.24	612	1.73	10	0.04	397	
M-17	4555.8	16.6	16.49	40.36	56.85	243	0.48	3	0.29	416	
M-03	4574	9.9	5.77	69.69	75.46	704	1.02	10	0.08	400	
M-04	4604	10.5	5.25	58.68	63.93	559	1.1	10	0.08	398	
M-05	4614	16.5	9.06	97.34	106.40	590	1.7	10	0.09	395	
M-06	4634	16.1	5.16	100.99	106.15	627	1.59	10	0.05	398	
M-20	4634.8	13	6	85.48	91.18	655	1.11	9	0.07	398	
M-07	4654	8.66	9.2	64.83	74.03	749	0.6	7	0.12	412	
M-08	4674	11.9	7.87	96.05	103.92	807	1.37	12	0.08	398	
M-22	4676	18.3	4.85	111.29	116.14	608	1.81	10	0.04	394	
M-09	4693	14.2	2.75	78.97	81.72	556	1.24	9	0.03	397	
M-10	4700.3	19.3	4.65	95.68	100.33	496	1.89	10	0.05	395	
M-11	4774	10.6	8.59	77.57	86.16	732	1.27	12	0.10	402	
M-23	4791	7.99	5.03	53.49	58.52	669	0.73	9	0.09	407	
M-12	4793	5.49	2.68	30.1	32.78	548	0.5	9	0.08	406	
M-13	4804	17.4	9.37	120.06	129.43	690	1.61	9	0.07	405	
M-14	4828.8	8.73	3.69	59.28	62.97	679	0.71	8	0.06	406	
M-25	4830	12.8	7.89	105.89	113.78	827	1.35	11	0.07	404	
M-15	4854.8	1.65	1.23	10.15	11.38	615	0.25	15	0.11	407	
M-30	4856	2.63	1.95	17.83	19.78	678	0.38	14	0.10	408	

Table 2: The rock-eval pyrolysis data of the studied section

Rock-Eval pyrolysis yielded  $T_{\max}$  values of 391-416°C, indicative of thermal immaturity for oil generation (Table 2). These  $T_{\max}$  values corroborate with  $T_{\max}$  values from Curiale and Odermatt (1989) of 390-412 °C. The organic matter type in these samples is determined with the cross-plotting of the hydrogen index and oxygen index, normally represented in a van Krevelen H/C versus O/C diagram, Figure 5. The hydrogen index (HI) is a proxy for atomic H/C calculated by  $([100 \cdot S_2]/\text{TOC})$  and is a measure of the quantity of hydrogen in kerogen. The oxygen index (OI) is a proxy for atomic O/C calculated by  $([100 \cdot S_3]/\text{TOC})$  and is a measure of the quantity of oxygen in kerogen. Remains of carbohydrate-rich land plants and inert organic matter typically have a much higher OI than marine sediments. Marine sediments are generally composed of proteins and lipid-rich organic matter that have a relatively higher proportion of hydrogen than land plants. The samples in this study have a substantially higher HI than OI, and all identify as Type I (marine sourced) kerogen.

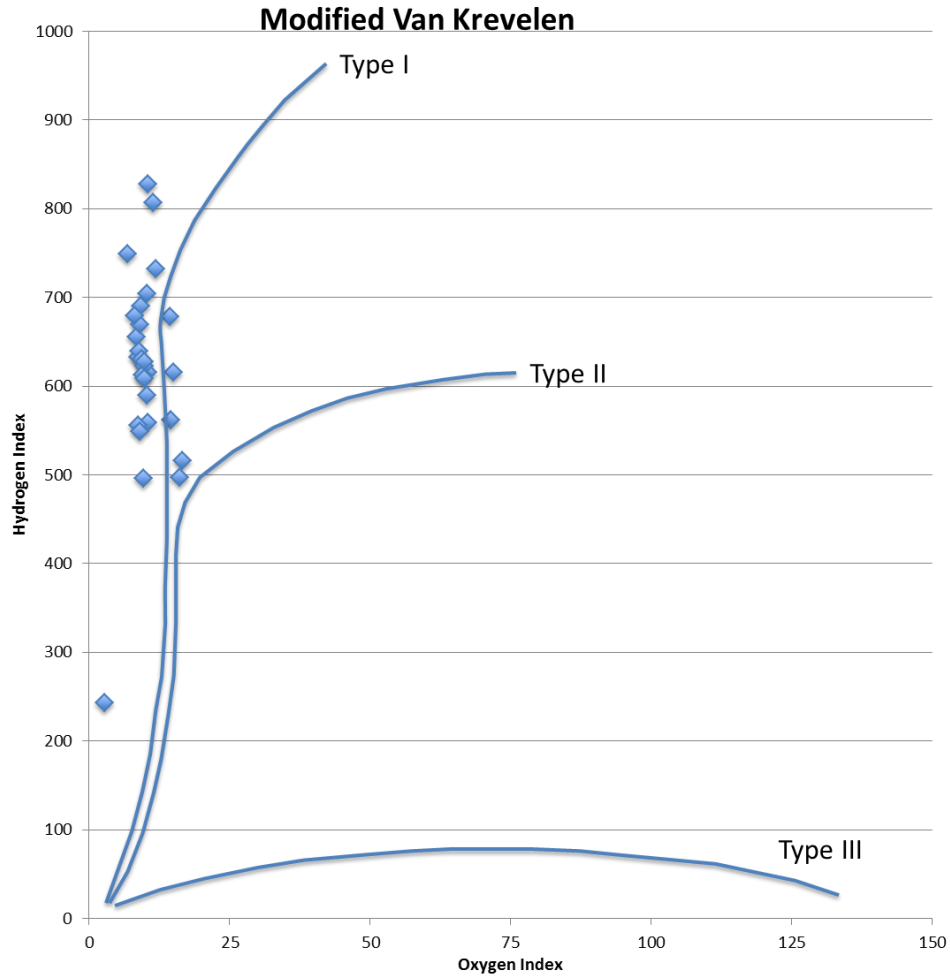


**Figure 6: Modified van Krevelen diagram. All data points are Type I kerogen, and all but one are immature.**

Cross-plotting of HI and OI can also help estimate thermal maturity. Samples lose H and O relative to C during burial and thermal maturation, and follow the paths of the van Krevelen diagram as maturity increases. The HI (243-807 mgHC/gTOC) and the OI (3-17 mgCO<sub>2</sub>/gTOC) data for the Monterey samples in this study show that they're thermally immature Type I kerogen, consistent with prior studies of this core (Curiale and Odermatt 1989).

## 1.6. Discussion

### 1.6.1. $^{187}\text{Re}$ - $^{187}\text{Os}$ Geochronology

Regression of all  $^{187}\text{Re}$ - $^{187}\text{Os}$  isotope data from this study produced a Model 3 age of  $11.5 \pm 1.5$  Ma (13% age uncertainty,  $2\sigma$ ,  $n=28$ , mean square of weighted deviates [MSWD] = 112), which agrees within uncertainties of the expected age of the Serravallian Monterey from prior studies of Curiale and Odermatt (1989) and others (Figure 3, see Geologic Setting). The calculated  $(^{187}\text{Os}/^{188}\text{Os})_i$  (using  $\lambda=1.666 \times 10^{-11}\text{a}^{-1}$ ; Smoliar et al., 1996) at 11.5 Ma for all samples ranges from  $0.713 \pm 0.030$  to  $0.859 \pm 0.005$  (average uncertainty of 0.8%,  $2\sigma$ ,  $n=28$ ), with an average  $(^{187}\text{Os}/^{188}\text{Os})_i$  of 0.78 (Table 1). There is not a clear stratigraphic correlation between facies,  $(^{187}\text{Os}/^{188}\text{Os})_i$ , and depth (Figure 6). An average uncertainty of 0.006% suggests that the minor  $(^{187}\text{Os}/^{188}\text{Os})_i$  variation between samples in Figure 6 accurately reflects the data and is not due to analytical uncertainty. The minor  $(^{187}\text{Os}/^{188}\text{Os})_i$  variability with both facies suggests that basinal Os input didn't vary much through deposition of both facies in the sampled section. These large uncertainties in age and the large MSWD value are consistent with the scatter about the isochron being controlled by geological factors, versus purely analytical uncertainties. The large uncertainty in age can be attributed to the large stratigraphic sampled interval, as a continuously sampled ~350-foot interval represents about 1.1 million years of Monterey deposition (Mackinnon, 1989). Calculated Model 3 ages assume the scatterchron is not a result of analytical uncertainty and incorporates geologic factors, such as post depositional mobility of Os or a change in  $(^{187}\text{Os}/^{188}\text{Os})_i$  (Ludwig, 2008).

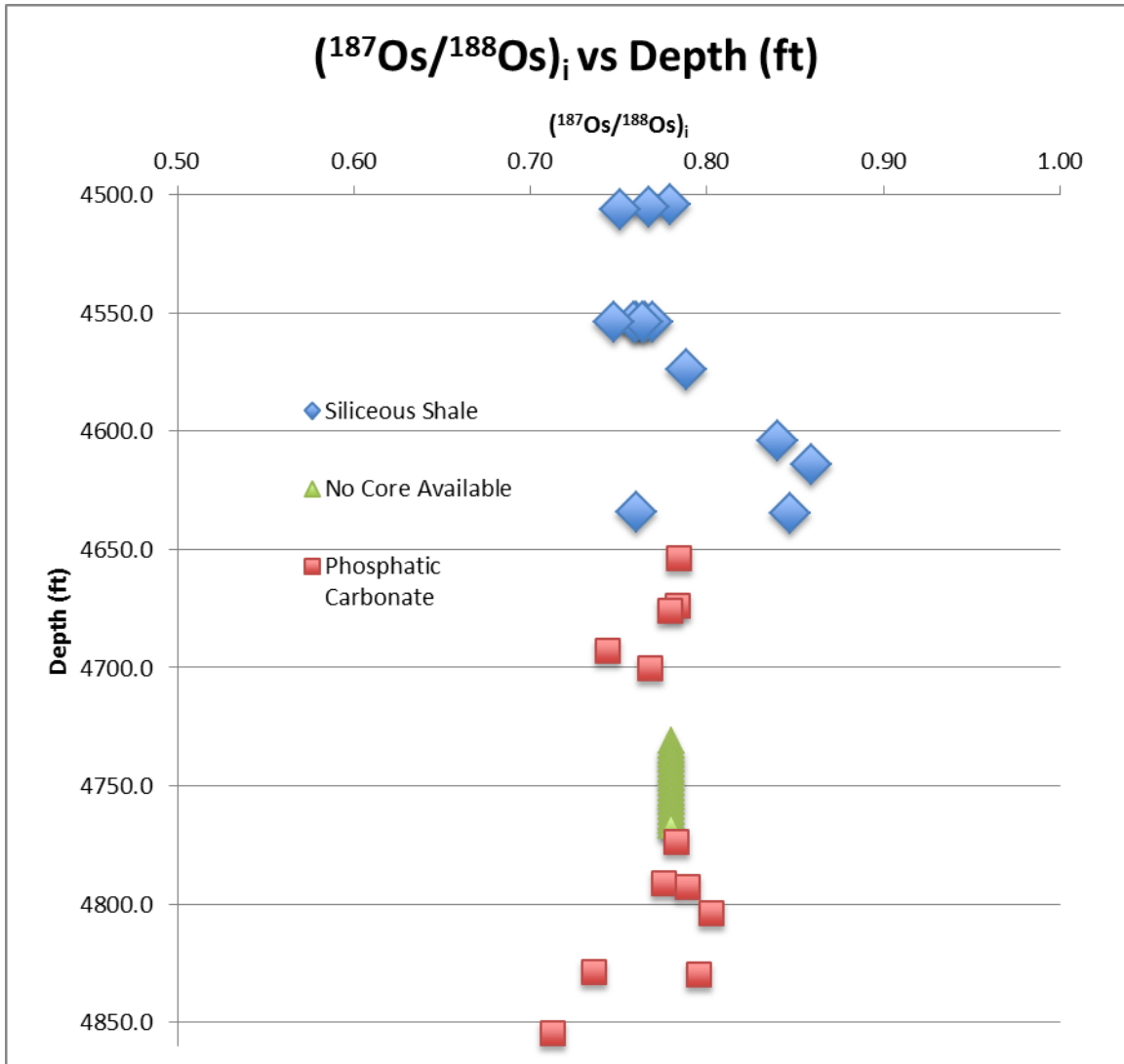


**Figure 7:**  $(^{187}\text{Os}/^{188}\text{Os})_i$  plotted against depth. There isn't a significant change as depth increases or between facies for  $(^{187}\text{Os}/^{188}\text{Os})_i$ .

### 1.6.2. Comparison to established age

With the long oil-producing history of the Monterey in California, the Monterey Formation and the Santa Maria basin have been extensively studied. However, there are no previously reported absolute ages for the Serravallian Monterey using  $^{187}\text{Re}$ - $^{187}\text{Os}$  geochronology. The age of  $11.5 \pm 1.5$  Ma agrees within uncertainty of the defined Serravallian

Miocene (Gradstein and Ogg, 2012). Bentonite and benthic foraminifera studies have aided in identifying various aspects of Monterey history, and provide an approximate age framework, as mentioned above.

Three conditions must be met to obtain precise and accurate isochron ages. 1) There must be a significant spread in measured  $^{187}\text{Re}/^{188}\text{Os}$ , which results from a large spread of  $^{187}\text{Re}/^{187}\text{Os}$ . 2) The initial seawater conditions of  $(^{187}\text{Os}/^{188}\text{Os})_i$  had to be consistent for all samples evaluated. 3) There cannot be any post depositional mobilization of Re or Os; it needs to remain a closed system. This study's  $^{187}\text{Re}/^{188}\text{Os}$  range of 634-2164 is sufficient whereas the  $^{187}\text{Os}/^{188}\text{Os}$  range of 0.88-1.18 isn't quite ideal for statistical minimization of uncertainties for age calculations.

### **1.6.3. Re and Os Uptake and Fractionation in Restricted Basinal Systems**

Definitive controls of Re and Os uptake and fractionation in ORM are still being determined. In this section, what has been constrained to present is reviewed. An examination of the data obtained in this study in the context of how Re and Os uptake is related to the organic material within the samples is integrated into this discussion in order to constrain what governed the abundances of these elements within the Monterey section studied.

Early studies on Re and Os uptake in organic-rich rocks have shown that for efficient uptake of these elements, sub-oxic to anoxic conditions must exist at or below the sediment water interface (Cohen et al., 1999; Colodner et al., 1993; Crusius et al., 1996; Koide et al., 1991; Morford and Emerson, 1999). These studies demonstrate that Re and Os have varying behaviors in the water column, with different uptake fractionation mechanisms (Levasseur et al., 1998; Selby et al., 2009). Soluble Re ( $\text{Re}^{\text{VII}}\text{O}_4^-$ ) is removed from seawater by reductive capture during diffusion into anoxic pore waters, and under low oxidation potential (Eh) conditions is converted to the insoluble form of  $\text{Re}^{\text{IV}}$  (Colodner et al., 1993). It has been suggested that soluble Os ( $\text{Os}^{\text{IV}}$ )

is removed from seawater due to a direct association with presence of organic matter (Yamashita et al., 2007). The removal rate of Os from seawater is therefore controlled by organic matter, and also affected by sediment accumulation rates and redox conditions. The slower the depositional rate of the studied interval the more enhanced Os uptake appears to be (Selby et al., 2009; Rooney et al., 2012). By comparison, Re removal from seawater appears to be unaffected by changes in sediment accumulation rate (Crusius and Thompson, 2000). A slower depositional rate conflicts with ideal TOC preservation due to a longer residence time for organic matter oxidation (Ibach, 1982).

Previous studies have also questioned the premise that Re and Os abundances are directly correlated to TOC (Cohen et al., 1999). Older studies such as Cohen et al. (1999) used inverse aqua-regia instead of the Jones Regent. Aqua regia oxidizes both hydrogenous and non-hydrogenous organic matter, and a correlation involving Re and Os abundances with TOC isn't likely. Other studies with questionable correlations between Re and Os and TOC were performed on ORMs from restricted basins (MacArthur et al., 2008; Baioumy et al., 2011; Cumming et al., 2012).

MacArthur et al. (2008) presented molybdenum (Mo) data plotted against TOC from the Cleveland Basin (United Kingdom) during the Toarcian (Jurassic) period, and compared it to existing Re and Os versus TOC datasets from Cohen et al. (1999). Molybdenum concentration is a useful indicator of paleoredox in organic-rich sediments. The slopes of two Mo versus TOC regression lines defined two periods of water mass restriction, which was supported by a negative excursion in  $\delta^{13}\text{C}_{(\text{org})}$  recorded in the same sediments (Figure 7, MacArthur, 2008). The lower half of their subzone had a Mo/TOC regression slope of 0.5, indicating extreme restriction, whereas the overlying subzone had a Mo/TOC regression slope of 17. Both of these values are at extremes compared to modern-day, open seawater Mo/TOC regression slope of 4.5 (MacArthur,

2008). The overlying subzone with a Mo/TOC regression slope of 17 was shown to be comparable to the Cohen et al. (1999) data where both the Re/TOC and Os/TOC slope regressions had similar slopes indicating minimal amounts of restriction. Baioumy et al. (2011) reported  $^{187}\text{Re}$ - $^{187}\text{Os}$  isotope data from Egypt where the laterally correlated marine shales and coals showed a strong positive correlation between TOC and Re and Os abundances ( $R^2 = 0.87$  and  $0.89$ , respectively), compared to laterally correlated non-marine shales and coals ( $R^2 = 0.19$  and  $0.37$ , respectively). Cumming et al. (2012) reported a weak correlation between TOC and Os in the proximal and distal lacustrine deposits in the Green River Basin, with  $R^2$  values of  $0.56$  and  $0.41$  respectively. These distal and lacustrine deposits of the Douglas Creek member were deposited on a lake margin, making them more susceptible to fluctuating water levels and subsequent sedimentation rates. By comparison, the zone deposited in the lake center exhibited a positive correlation between TOC and Re ( $R^2=0.73$ ). Slow sedimentation rates and consistent high water levels were attributed to a consistent rate of Re and Os uptake, leading to a stronger association of Re and organic matter.

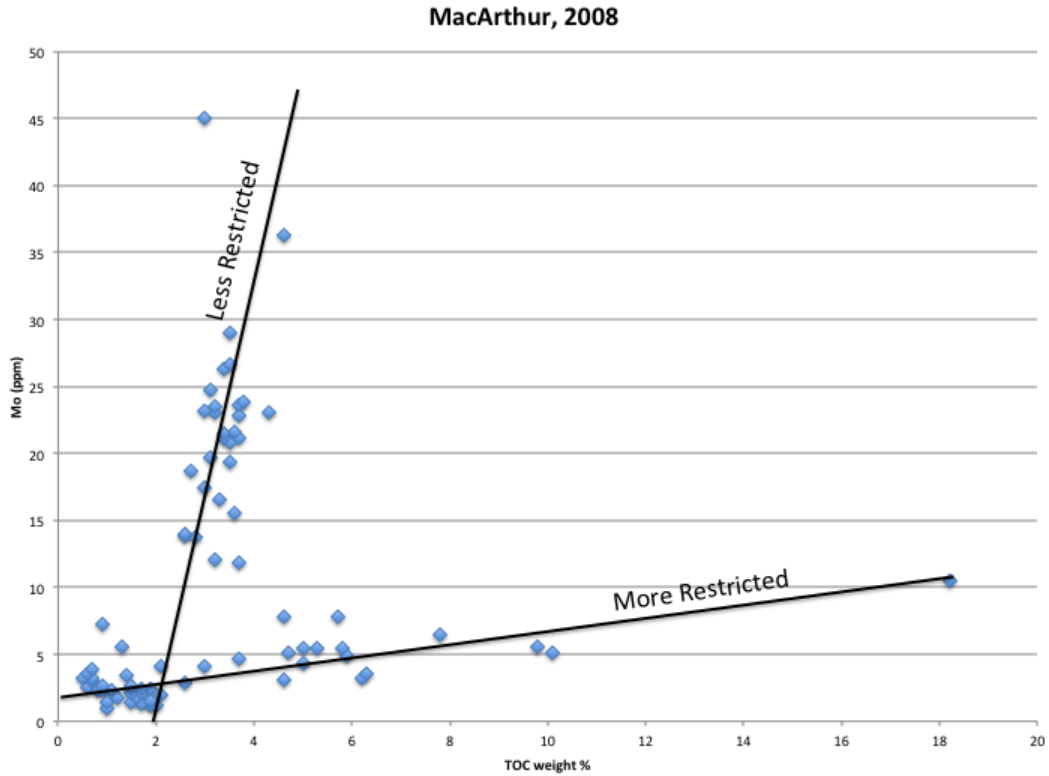


**Figure 8: TOC/Mo data from MacArthur 2008 to show correlation between slope of TOC/Mo and known restriction at time of deposition.**

The slope of correlated trend lines of TOC versus Re or TOC versus Os suggests a relationship with the sedimentation rate at time of deposition. The TOC preservation is related to sedimentation rates. A slower sedimentation rate leaves organic matter more exposed to biodegradation and oxidation, leading to smaller TOC values than was originally deposited. The other consequence of a slower sedimentation rate is the longer interaction time between Re and Os in seawater complexing with organic matter, thus leading to higher Re and Os abundances in ORM. Plotting higher Re and Os abundances against lower TOC values results in a high slope on a cross plot, representing a slow sedimentation rate. In contrast, a higher sedimentation rate increases organic matter preservation and shortens the amount of time that Re and Os have in

complexing with organic matter at the sediment-water interface. TOC preservation is affected by more than sedimentation rates, however, as basin restriction, stratification, water depth, and aforementioned diagenetic processes also affect TOC preservation. Macarthur (2008) suggested that in restricted basins, organic matter sedimentation draws down dissolved Re and Os from the water column, resulting in a shortening of Re and Os residence times. The shortening in residence times causes rapid variations in the availability of those elements in the water column, and ultimately results in rapid variations in the  $(^{187}\text{Os}/^{188}\text{Os})_i$  of sediments. Georgiev et al. (2011) also reported a positive correlation between TOC and molybdenum abundance and basin restriction. The paleoredox similarities between molybdenum and Re and Os in comparison with TOC reinforce using TOC with Re and Os as a metric in evaluating basin restriction at time of deposition.

As seen in Figure 9A, both of this study's facies have similar slopes of TOC versus Re for siliceous-shale and phosphatic-carbonate, with slopes of 15.3 and 10.2, respectively, that correlate well with the late Cretaceous marine shale of Baioumy et al. (2011). The differences in Os versus TOC for the two facies are even more pronounced, with slopes of 69.5 and 36.8 for the phosphatic-carbonate and siliceous-shale, respectively, shown in Figure 9B. In plotting TOC vs Os as well, the slope difference based on depositional environment sorts out the facies restriction at time of deposition appropriately. The depositional differences shown by TOC versus Os and Re plots support the argument about using the slope of TOC/Mo data as well.

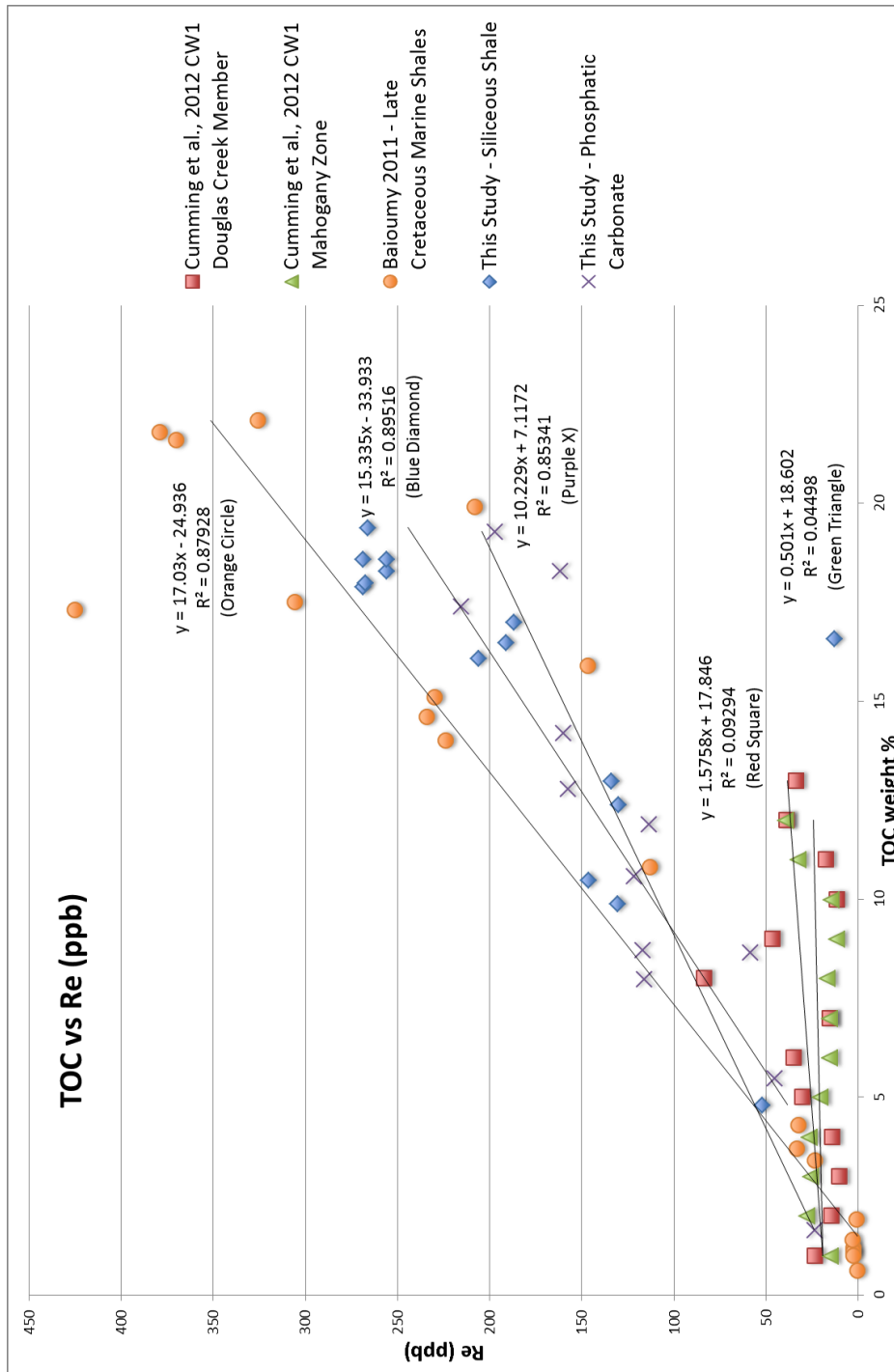


**Figure 9A: TOC vs Re abundances of this study, plotted against TOC vs Re abundances from other studies. Baioumy et al., 2011, shows the slope of a marine shale. Both facies from Cumming et al., 2012, are distal and proximal lacustrine shales.**

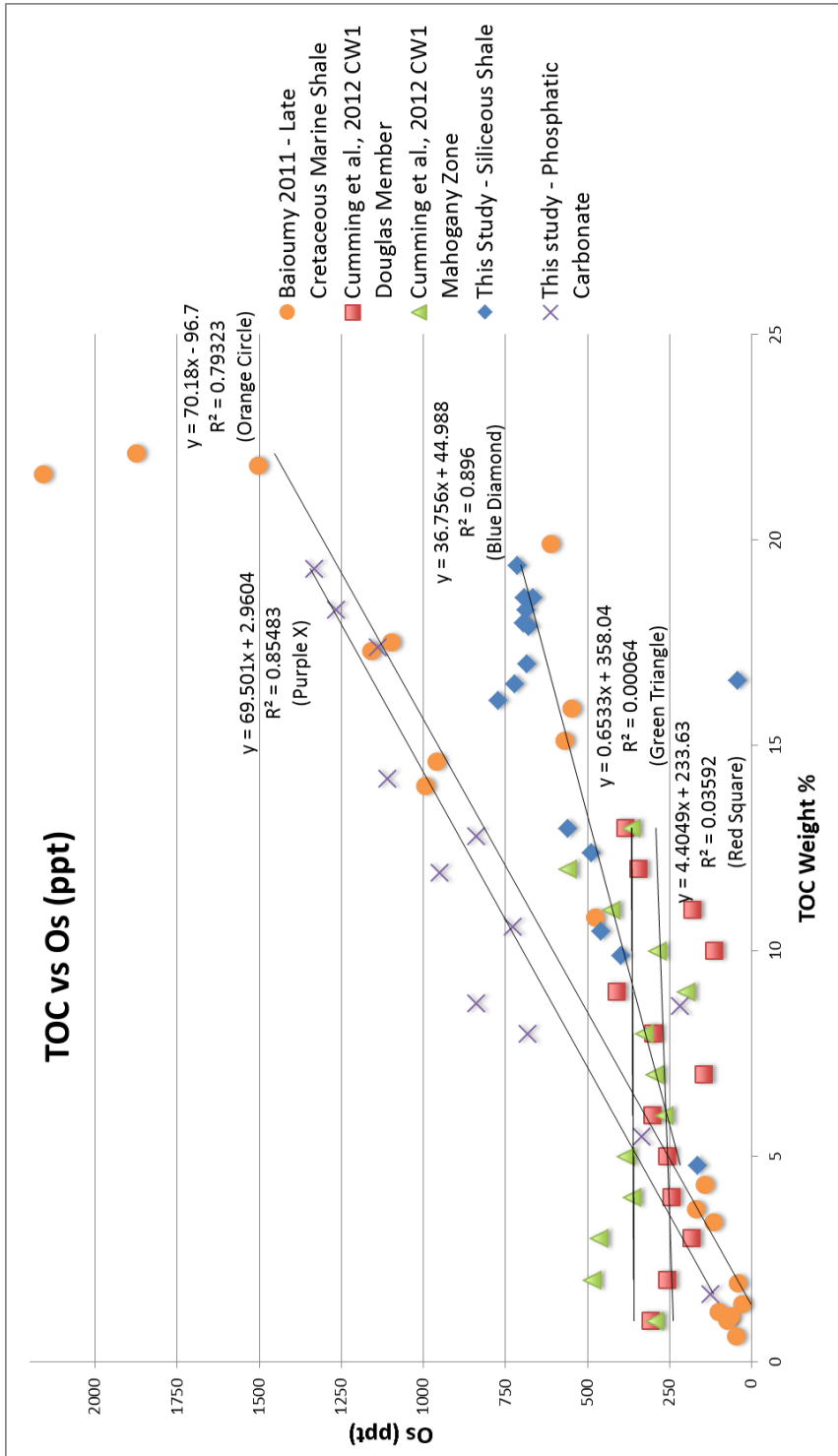


Figure 9B: TOC vs Os abundances of this study, plotted against TOC vs Os abundances from other studies. Baioumy et al., 2011, shows the slope of a marine shale. Both facies from Cumming et al., 2012, are distal and proximal lacustrine shales.

#### 1.6.4. TOC with depositional conditions

Both the siliceous-shale and phosphatic-carbonate facies exhibit a linear correlation of Re and Os versus TOC (Figure 9). The phosphatic-carbonate facies have a correlation for Re versus TOC with  $R^2$  of 0.844 and for Os versus TOC with  $R^2$  of 0.814, with slopes of 10.5 and 72.5, respectively. The siliceous-shale facies doesn't correlate as well in Os versus TOC with an  $R^2$  of 0.412 and a Re versus TOC with  $R^2$  of 0.511, with slopes of 36.8 and 15.3, respectively (Figure 9). However, there is one outlier siliceous-shale data point (M-17) on both charts significantly affecting correlations. Results excluding the outlier M-17 are shown in Figure 10. The siliceous-shale's correlation with TOC, Re and Os significantly improved to 0.895 and 0.896, respectively, and the slopes stayed the same.

The biggest difference in comparing both facies' relationships with Re, Os and TOC is the slope difference between facies when plotting TOC versus Os. The phosphatic-carbonate has a higher slope (72.5) than the siliceous-shale (36.8), suggesting that the phosphatic-carbonate was deposited during a period of less restriction when compared with the siliceous-shale. This supports the depositional setting laid out by Mackinnon (1989) that the phosphatic-carbonate facies was deposited in a near-shore basin during a time of relatively less restriction and higher sea level compared with the siliceous-shale (See section 1.2. geologic setting). However, the varying degree of basinal restriction did not affect depositional rate, which was approximately 984 ft/m.y. for both facies in the study interval (Pisciotta and Garrison, 1981).

Climate is also a factor that affects depositional rates. The Miocene during this study's deposition was in an icehouse climate starting at 13.9 Ma, and had subsequent climate cycles lasting 100,000 years (Holbourn et al., 2007). Holbourn et al. (2007) used  $^{18}\text{O}$  and  $^{13}\text{C}$  isotopes to evaluate orbitally-paced climate evolution (Milankovitch Cycles) to determine the cycle length.

Using the depositional rate of 984 feet/m.y. the core interval of this study represents approximately 350,000 years, which is a large enough range to potentially see Miocene climate cyclicity, and specifically how it affects seawater ( $^{187}\text{Os}/^{188}\text{Os}$ )<sub>i</sub>. However, the sporadic distribution of ( $^{187}\text{Os}/^{188}\text{Os}$ )<sub>i</sub> with no clear cycles through time shows that the Milankovitch cycles of the Miocene aren't directly reflected in ( $^{187}\text{Os}/^{188}\text{Os}$ )<sub>i</sub>. This could be attributed to a small-scale climate change within the 100,000 year climate cycles that didn't affect seawater osmium enough to show up in the rock record.

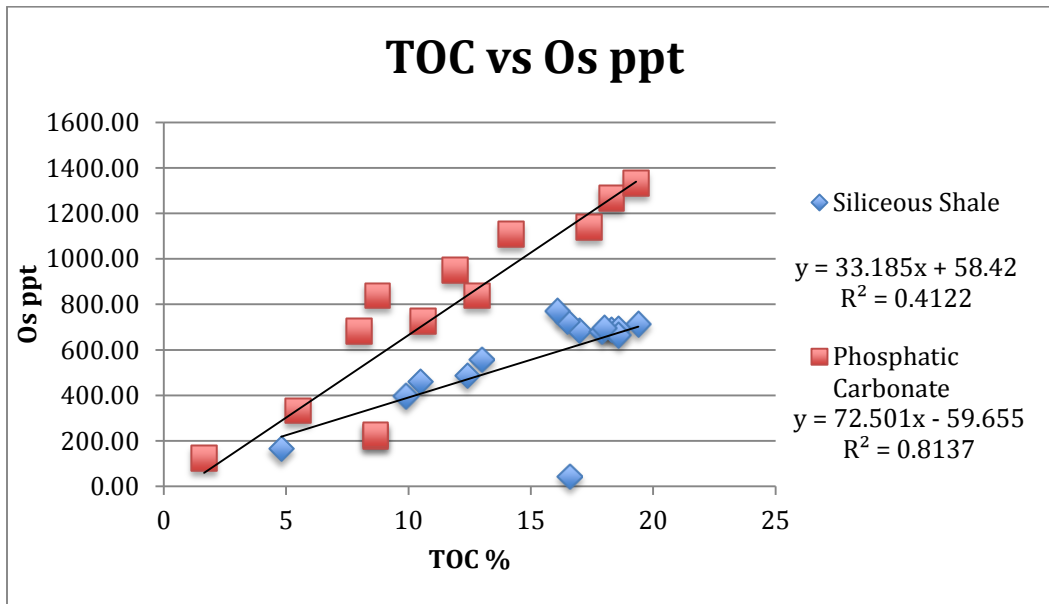
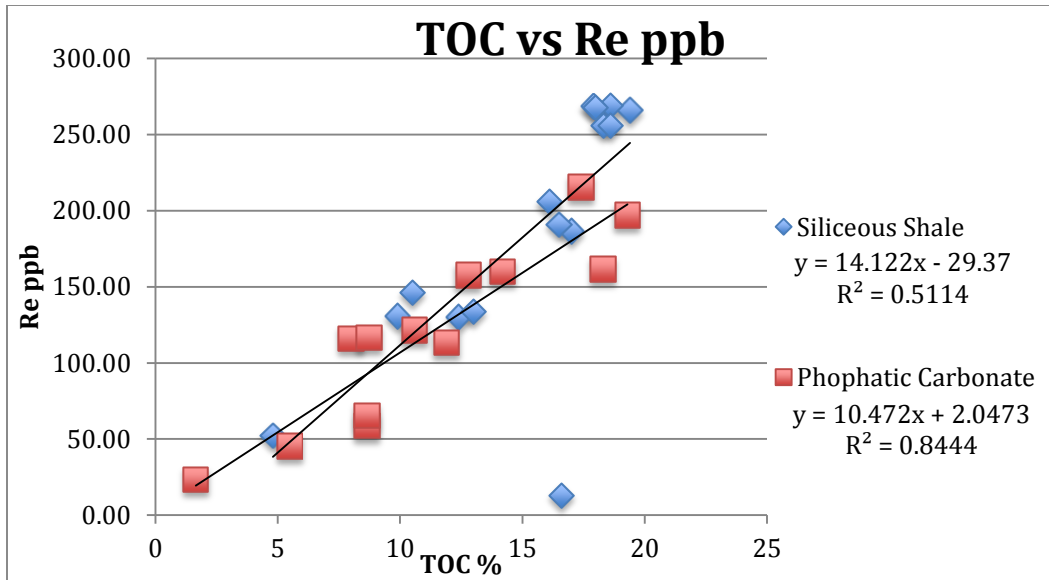


**Figure 10: TOC versus Re and Os, respectively. Note the differences in  $R^2$  between the facies with the one siliceous-shale outlier point (M-17).**

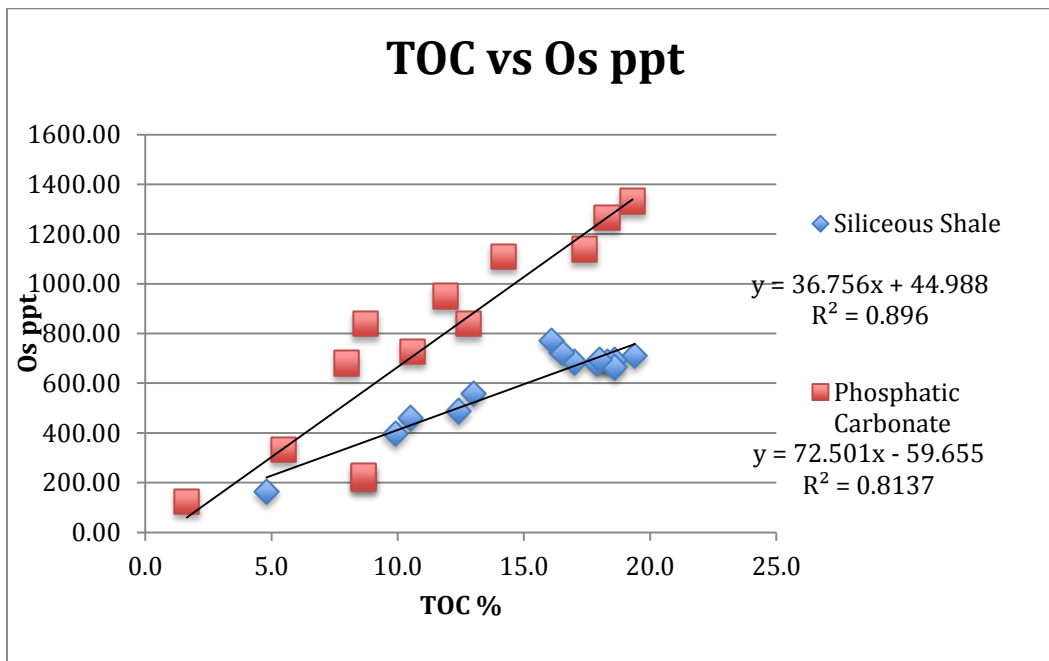
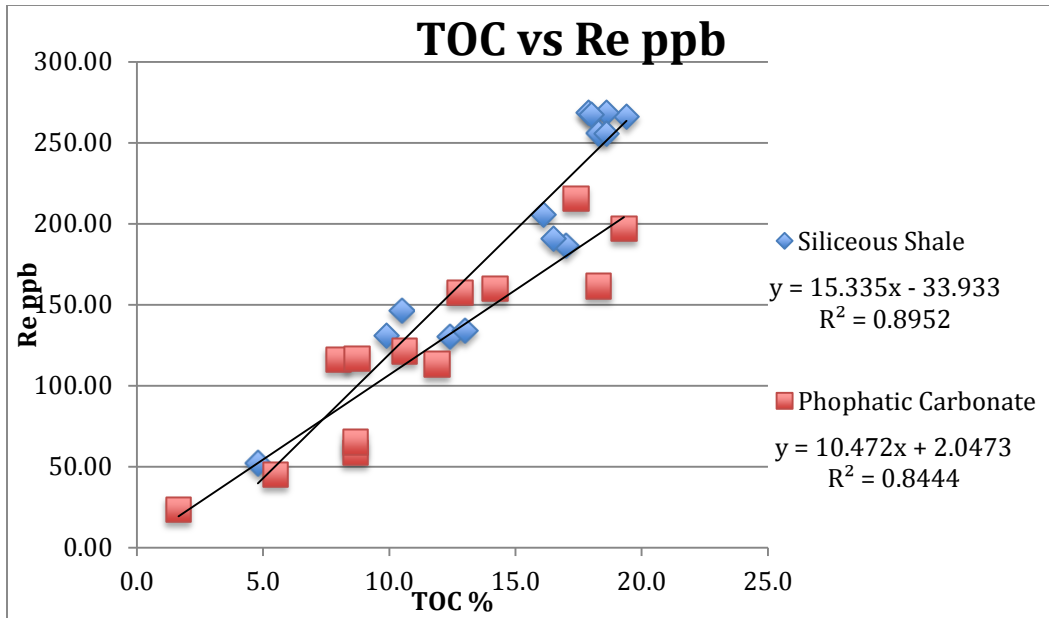


**Figure 11. TOC versus Re and Os, respectively, without the outlier siliceous-shale point (M-17). Note the similarities in  $R^2$  between the facies, and that the  $R^2$  for both elements is very similar as well.**

### 1.6.5. Effects of Organic Matter Type

The relationship between Re, Os, TOC, and depositional environment emphasizes that the type of organic matter may likely aid in influencing Re and Os uptake and fractionation. Since all samples in this study have similar  $T_{\max}$  values that indicate the section is thermally immature, oxygen index (OI) and hydrogen index (HI) values from Rock-Eval pyrolysis are used to better evaluate the type of kerogen present (Table 2). Curiale and Odermatt (1989) evaluated this core section using a modified van Krevelen diagram, and their data shows a possible mixture of Type I and Type II kerogen, though predominantly Type I (Figure 11). To appropriately compare this study's data to Curiale and Odermatt (1989) data, the Curiale and Odermatt (1989) data points shown in Figure 11 were selectively chosen from the exact interval (to the foot) that this study's data points was sampled from. There is a wide range of Type I and Type II kerogen presented in Curiale and Odermatt (1989) and limiting what's presented in Figure 7 to what directly compares with this study's data shows how similar the two data sets are. In this study all of the samples analyzed are Type I kerogen (Figures 5, 11). The samples chosen for this study were chosen from core locations with high TOC content as previously identified from the Curiale Odermatt (1989) study. Hence, it appears that the data obtained for this study is selectively filtered to be Type I kerogen. This is consistent with a lacustrine source for the organic matter and with minimal terrigenous organic matter input, and also supports previous observations that the TOC-enriched portions of the Monterey were deposited in a near-shore restricted basin environment (Mackinnon, 1992).

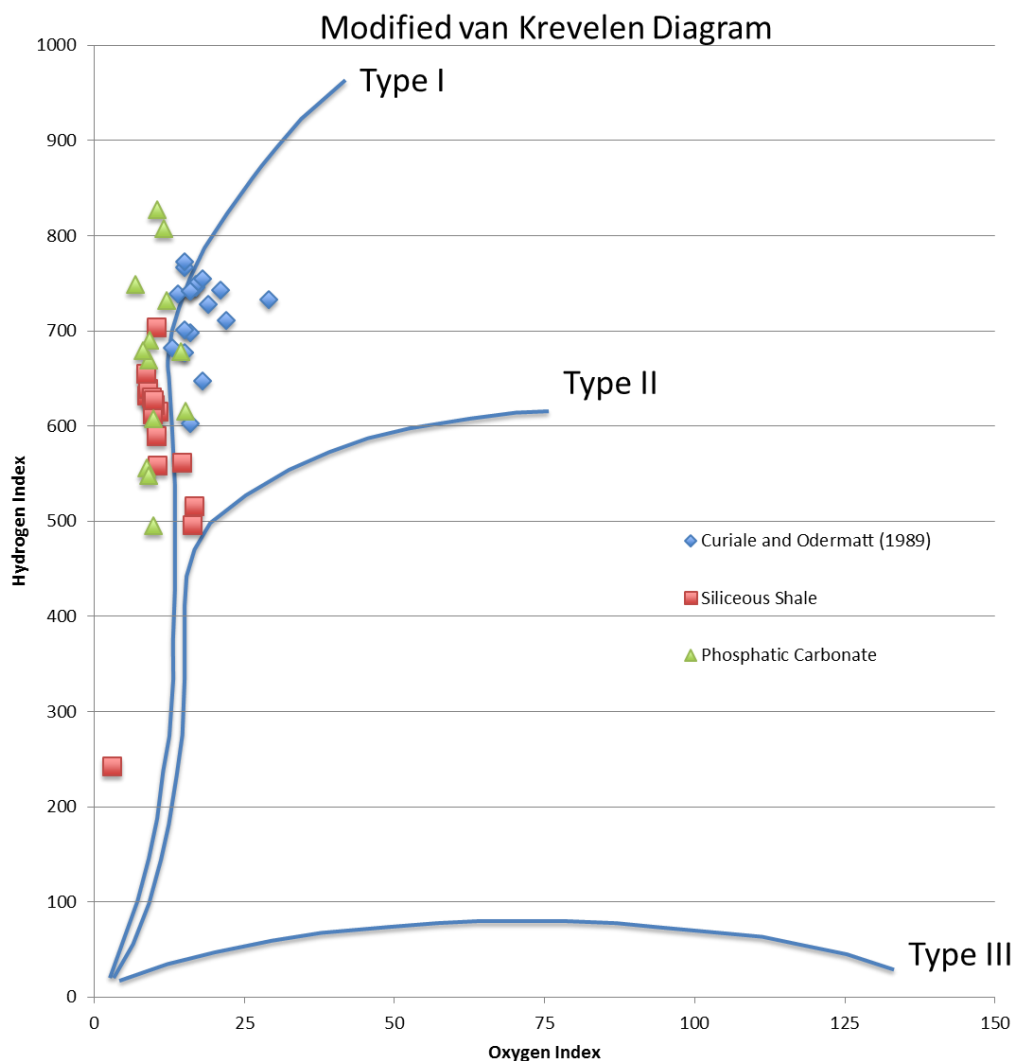


**Figure 12: Modified van Krevelen Diagram with selected data points from Curiale and Odermatt (1989) and this study. Note how almost all data points are Type I kerogen.**

As noted above in the Results section, Hydrogen Index (HI) is a proxy of Hydrogen content in kerogen, which in turn is dependent upon the type of organic matter at time of deposition. The Re and Os abundances versus HI do not display a correlation for the phosphatic-carbonate facies, with  $R^2$  values of 0.003 and 0.03, respectively (Figure 12). This indicates that

Re and Os abundances for the phosphatic-carbonate facies are not dependent upon the amount of organically bound hydrogen in Kerogen. By comparison, the Re and Os abundances versus HI for the siliceous-shale facies have a decent positive correlation, with  $R^2$  values of 0.47 and 0.54, respectively (Figure 12).

This data is presented again in Figure 13 without the outlier data point, M-17, in an attempt to improve correlations between Re, Os and HI for the siliceous-shale. The correlations for Re and Os versus HI did not improve compared to the entire set, with  $R^2$  values of 0.214 and 0.177 for Re and Os, respectively (Figure 13). Regardless of which data set used to compare Re, Os and HI, the siliceous-shale has a much higher correlation than the phosphatic-carbonate.

The significant difference in correlation between the siliceous-shale and the phosphatic-carbonate with Re and Os versus HI suggests that Re and Os abundances are dependent upon the organically bond hydrogen in kerogen. This is also supported by the siliceous-shale having a higher average TOC of 15.2% (n=15) versus an average TOC of 10.7% (n=13) for the phosphatic-carbonate (Table 2, Figure 4). Based on Figure 12, it appears that both Os and Re best complex with HI for both facies between 500 and 700 (mgHC/gTOC). In addition to the  $R^2$  differences between the facies, the variation in  $R^2$  values between Re and Os suggests that there are differences in the uptake mechanism between Re and Os, as Os sequestration is directly related to the presence of organic matter (Yamashita et al., 2007).

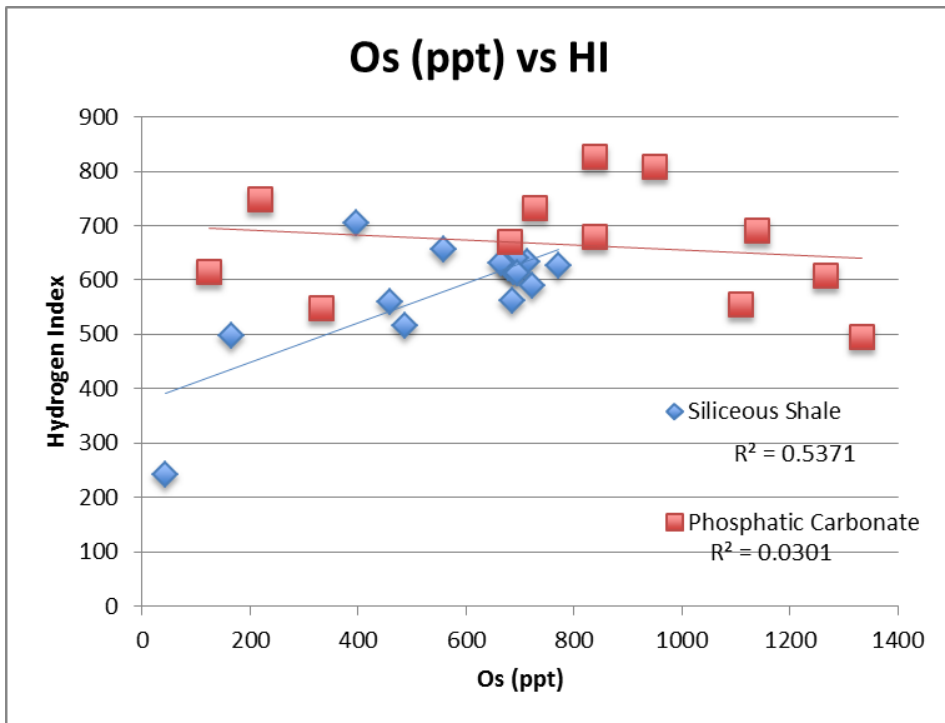
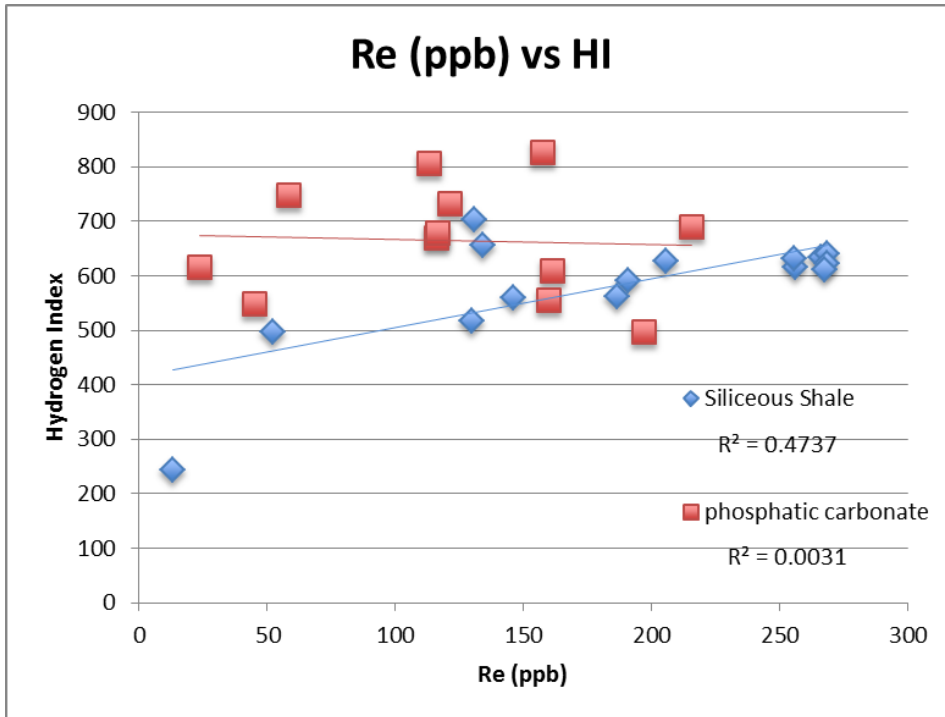


**Figure 13: Hydrogen Index plotted against Re (ppb) and Os (ppt), respectively. Note the low  $R^2$  values when compared to Re and Os versus TOC**

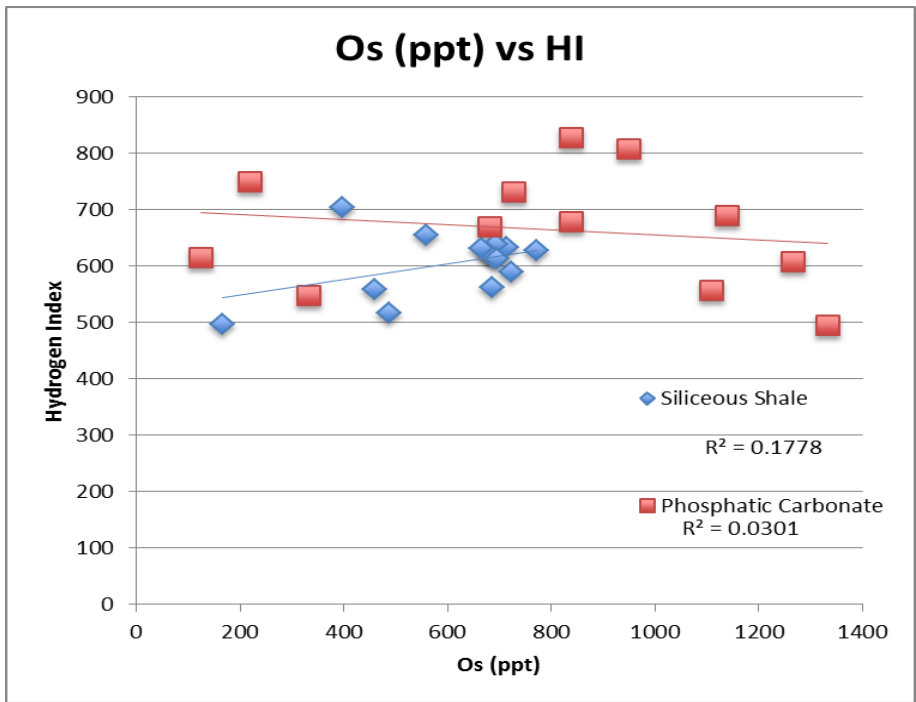
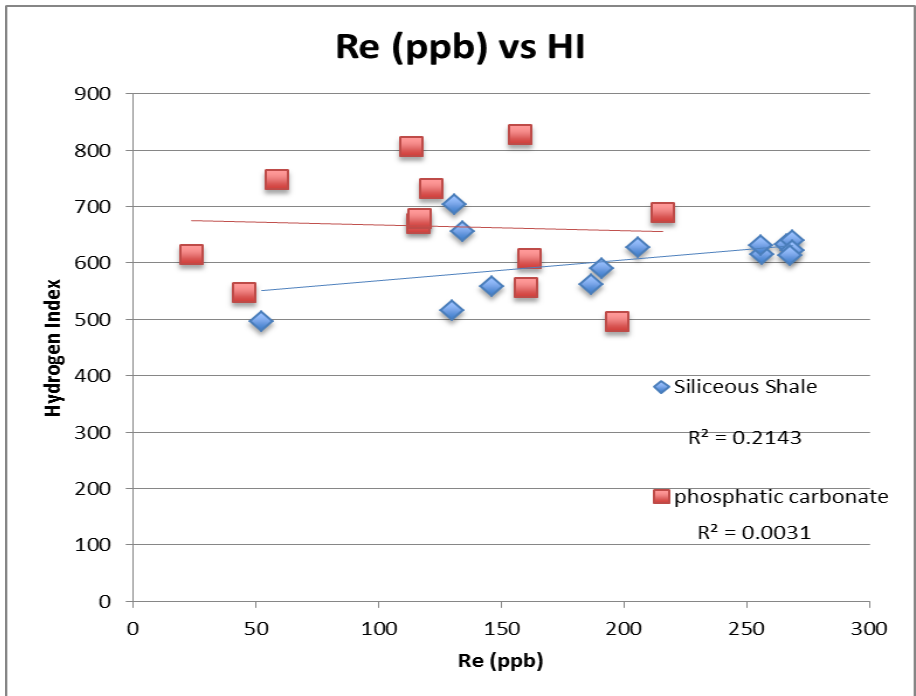


**Figure 14: Hydrogen Index plotted against Re (ppb) and Os (ppt), respectively. These two plots exclude the outlier point (M-17) to see how correlations for the siliceous-shale change. Correlations for the siliceous-shale between Re, Os and HI actually decrease when taking out M-17.**

Also noted above, Oxygen index (OI) is a proxy of oxygen content in kerogen, which is also dependent on the organic matter type preserved after deposition. There is no correlation between Re or Os versus OI for either the phosphatic-carbonate or siliceous-shale facies when plotting the entire data set. The phosphatic-carbonate facies have  $R^2$  values of 0.07 for Re versus OI, and 0.04 for Os versus OI, respectively (Figure 14). The siliceous-shale facies have  $R^2$  values of 0.001 for Re vs OI and 0.007 for Os versus OI, respectively (Figure 14). These correlations were also compared to a data set without the outlier M-17 (Figure 15) to see if  $R^2$  values improved for the siliceous-shale. Removing M-17 from the siliceous-shale data set yields  $R^2$  values of 0.389 for Re versus OI and 0.323 for Os versus OI (Figure 15). While the correlations are comparably higher without M-17, they're still weak on an absolute basis. This indicates that Re and Os abundances in both facies are not dependent upon the amount of organically bound oxygen in kerogen, and papers such as Cumming et al (2013) reported a non-correlation between Re, Os and OI as well. The relationship of Re and Os versus OI for both facies appears to preferentially complex between 7 and 12 (mg CO<sub>2</sub>/g TOC) regardless of Re or Os values.

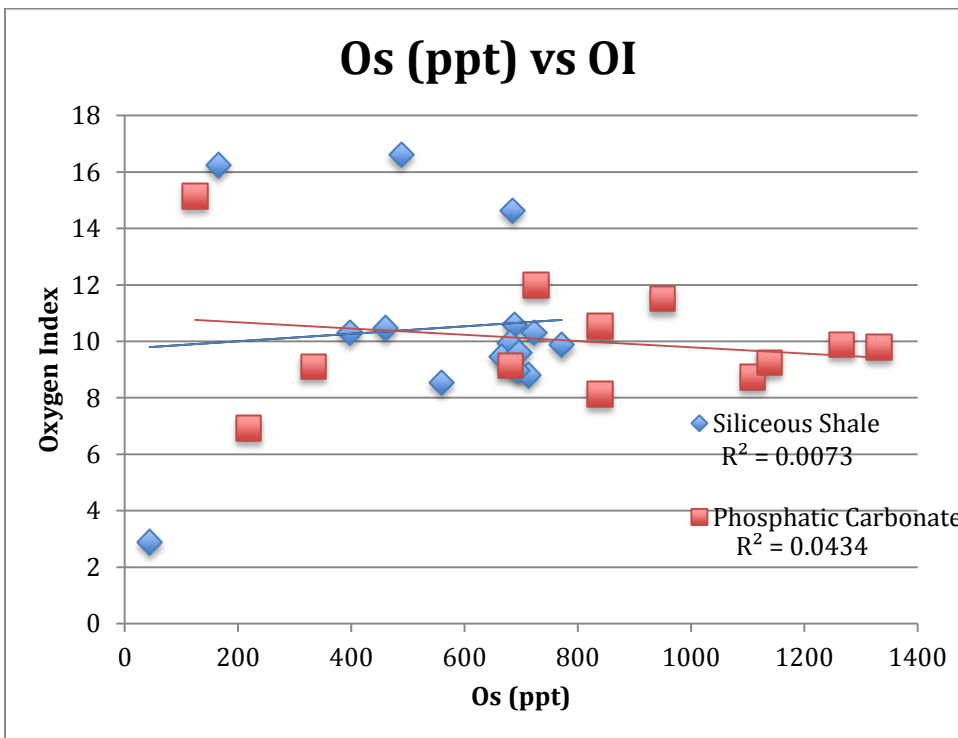
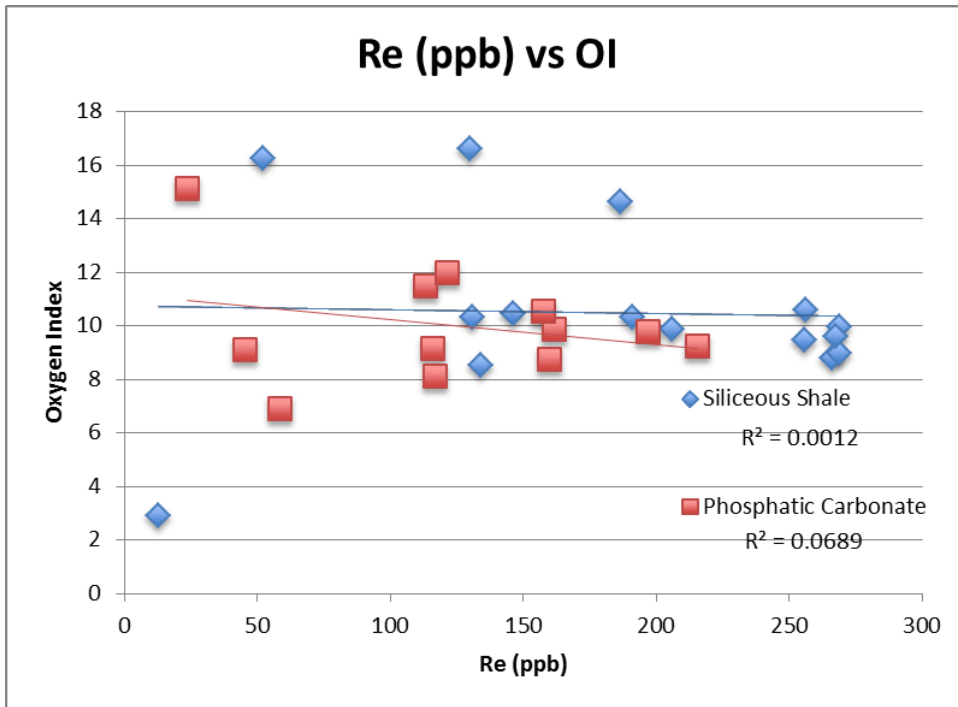


**Figure 15: Oxygen Index plotted against Re and Os. Note the lack of correlation in the relationship between both elements and facies.**

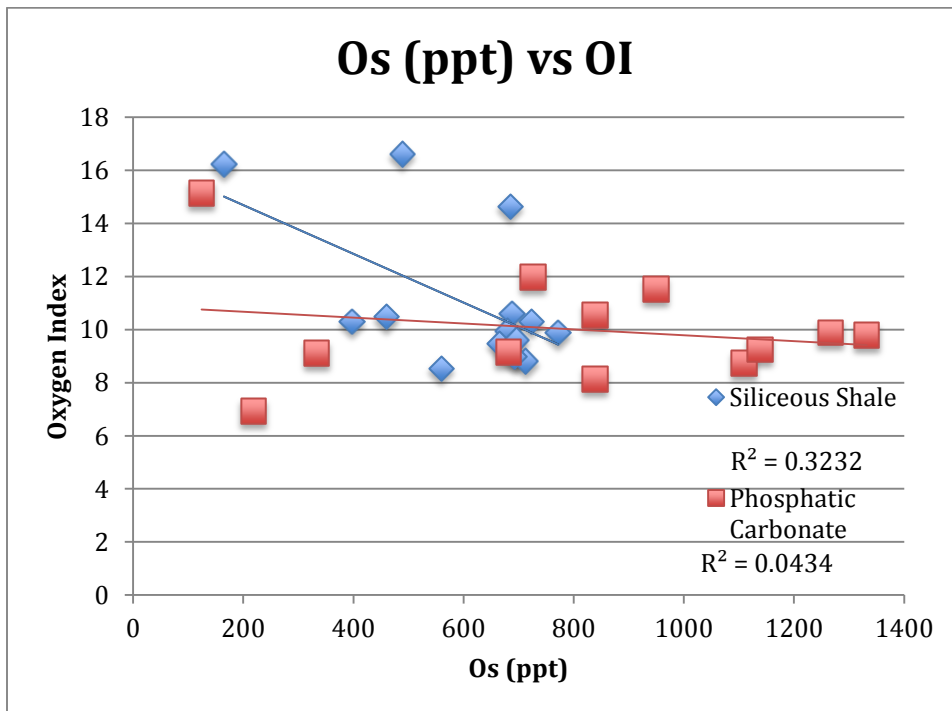
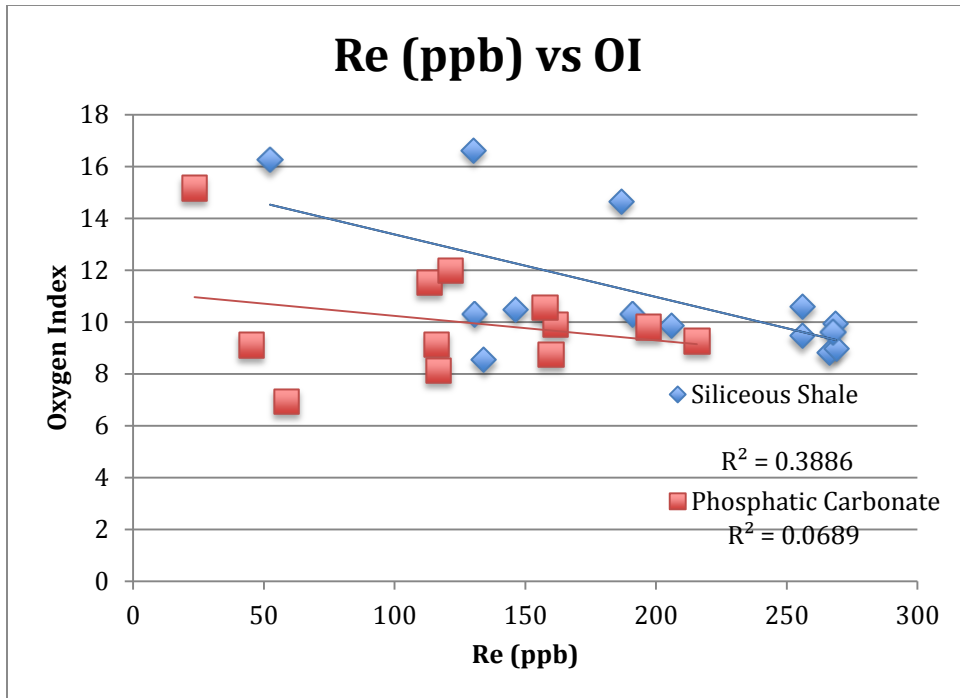


**Figure 16: Oxygen Index plotted against Re and Os, without the outlier M-17 sample. Note the correlation improvement between the siliceous-shale for both Re and Os versus OI.**  
**1.6.6. Os isotope implications of (<sup>187</sup>Os/<sup>188</sup>Os)<sub>i</sub> at 11.5 Ma**

The  $^{187}\text{Re}$ - $^{187}\text{Os}$  isotope data of the entire Monterey study section yields an average  $(^{187}\text{Os}/^{188}\text{Os})_i$  value of  $0.779 \pm 0.037$  ( $2\sigma$ ). The siliceous-shale facies has an average  $(^{187}\text{Os}/^{188}\text{Os})_i$  value of  $0.783 \pm 0.004$  ( $2\sigma$ ), and the phosphatic-carbonate facies has an average  $(^{187}\text{Os}/^{188}\text{Os})_i$  value of  $0.775 \pm 0.006$  ( $2\sigma$ ), respectively, both of which suggest a less-radiogenic composition of Os in the Santa Maria Basin water column when compared to the modern seawater  $(^{187}\text{Os}/^{188}\text{Os})_i$  value of 1-1.05 (Peucker-Ehrenbrink and Ravizza, 2012). The limited variance in average  $(^{187}\text{Os}/^{188}\text{Os})_i$  values between the two facies can be explained by the slight changes in basinal restriction between the two facies, as noted above, with the phosphatic-carbonate deposited in a slightly more restricted basin. The  $(^{187}\text{Os}/^{188}\text{Os})_i$  values for both Monterey facies fall in the middle of the accepted range of  $(^{187}\text{Os}/^{188}\text{Os})_i$  for mid-Miocene seawater of 0.75-0.85 as defined by Peucker-Ehrenbrink (2012). Hence, the Os within the water column of the Santa Maria basin was largely in equilibrium with the global oceans in the mid-Miocene.

The global ocean has become progressively more radiogenic in  $(^{187}\text{Os}/^{188}\text{Os})_i$  during the Cenozoic, ranging from 0.56 at 50 Ma to 1.05 present-day (Peucker-Ehrenbrink and Ravizza 2010). Sources of non-radiogenic Os into seawater include cosmic input, oceanic LIP basalts, and mid-ocean ridge hydrothermal input, and radiogenic Os is mostly sourced by runoff from continental crust. The development of inner and outer basins during transverse crustal block rotation (see Geologic Setting) mitigated the amount of radiogenic continental crust runoff into the Santa Maria Basin, leading to non-radiogenic seawater Os isotopic composition. There are macro-isotopic events both radiogenic and non-radiogenic from the Miocene that affected the oceanic Os budget in seawater such as the Columbia River Large Igneous Province (LIP) and the Nördlinger Ries meteorite impact (Klemm et al., 2008; Schmidt and Pernicka, 1994; Montanari and Koeberl, 2000).

The first event affecting seawater Os in the mid-Miocene was the Columbia River LIP in the Northwestern United States. The Columbia River LIP erupted 95% of its total flood basalt volume between 16.6 and 15.3 Ma (Courtilot and Renne, 2003; Klemm et al., 2008). Klemm et al. (2008) argued that there was a delay between flood basalt deposition and Os runoff into the Pacific Ocean from continental weathering of this material. This would have subsequently affected the  $(^{187}\text{Os}/^{188}\text{Os})_i$  in the Santa Maria Basin and Monterey Formation 3 to 4 million years later at the time of deposition (Figure 16). One could argue that the Columbia River LIP helped  $(^{187}\text{Os}/^{188}\text{Os})_i$  somewhat flat-line from 16.6 Ma to approximately 13 Ma, instead of becoming more radiogenic over that time period (Figure 16). However, it's a weak argument and would need to be supplemented with regionally adjacent cores from 16.6 Ma to 13 Ma, and that large of a flood basalt event would cause a significant  $(^{187}\text{Os}/^{188}\text{Os})_i$  incursion. The other Miocene event potentially affecting  $(^{187}\text{Os}/^{188}\text{Os})_i$  of the mid-Miocene is the Nördinger Ries meteorite impact. The Nördinger Ries meteorite impact in Germany occurred at  $15.1 \pm 0.1$  Ma and is the only known significant impact event between 5 and 24 Ma (Schmidt and Pernicka, 1994; Montanari and Koeberl, 2000). Klemm et al. (2008) argue that the Nördinger Ries impact supplemented Os from the Columbia River LIP's, resulting in the  $(^{187}\text{Os}/^{188}\text{Os})_i$  minimum excursion of 0.70 at ~12.5 Ma that is present in 3 cores throughout the Atlantic Ocean (Figure 16).

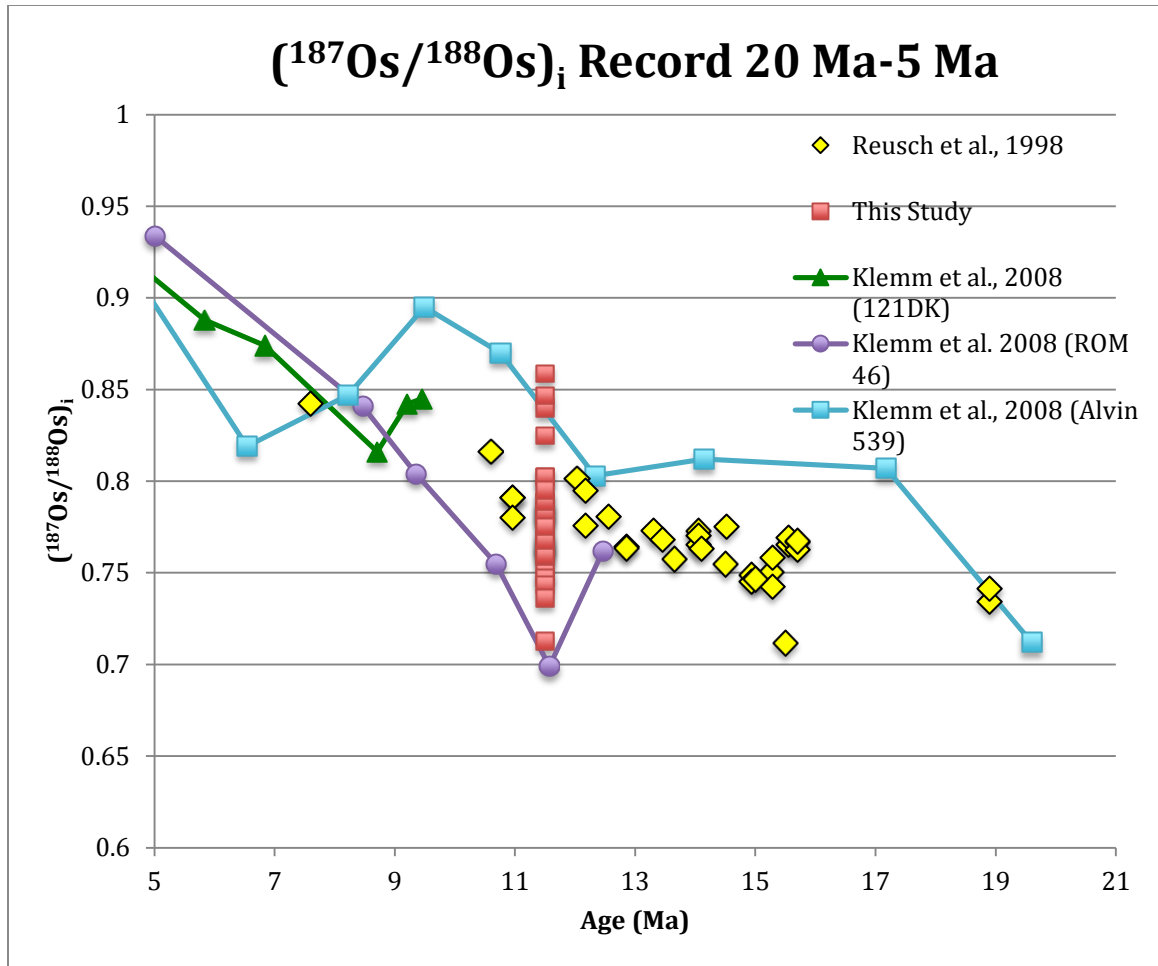


**Figure 17:  $(^{187}\text{Os}/^{188}\text{Os})_i$  record from 20 Ma to present, using studies highlighted by Peucker-Ehrenbrink and Ravizza, 2012. This study's samples fit right in the accepted range of mid-Miocene  $(^{187}\text{Os}/^{188}\text{Os})_i$  values.**

The fact that the Columbia River LIP's non-radiogenic  $(^{187}\text{Os}/^{188}\text{Os})_i$  contribution is observed in the Atlantic Ocean whereas its continental runoff went into the Pacific Ocean means that the drawdown to non-radiogenic Os should also be present in the Santa Maria Basin. Based on the minimal stratigraphic interval and time represented in this study it's hard to determine if the incursion is present. The 0.8% error from the  $(^{187}\text{Os}/^{188}\text{Os})_i$  data points in this study also suggests that the wide range of  $(^{187}\text{Os}/^{188}\text{Os})_i$  values reflects a small change in the balance of radiogenic versus non-radiogenic  $(^{187}\text{Os}/^{188}\text{Os})_i$  contribution to seawater. This is also reinforced

by the lack of trends in  $(^{187}\text{Os}/^{188}\text{Os})_i$  between depth (time) or a Monterey facies change, as either the Columbia River LIP or the Nördinger Ries impact would create trends. The combined  $(^{187}\text{Os}/^{188}\text{Os})_i$  averages of both facies in this study are still non-radiogenic at 0.78, but there's little conclusive evidence that the mid-Miocene  $\text{Os}_i$  minimum from the Columbia River LIP and Nördinger Ries crater are represented in this data set. Based on this study's age of  $11.5 \pm 1.5$  Ma, it's likely that this Os minimum excursion is stratigraphically below this study's interval or alternatively, does not exist. This needs further evaluation by examining multiple locales of the same age throughout the ocean sediment sequences and from peripheral basins.

### **1.7. Conclusion**

This study's goal was to accurately date the Monterey in this interval and examine Os isotope seawater values of the mid-Miocene, distinct sources of Os input, and how these relate to the depositional environments and source rock character of the Serravallian Monterey. The model age of  $11.5 \pm 1.5$  Ma is within the general accepted age of the Monterey and also supported from prior bentonite and biostratigraphic studies of Hornafius (2009). The  $(^{187}\text{Os}/^{188}\text{Os})_i$  values of this study interval also fall within the accepted Miocene  $(^{187}\text{Os}/^{188}\text{Os})_i$  values of seawater of 0.73-0.87  $\pm .005$  established by Peucker-Ehrenbrink and Ravizza (2010). The combination of a wide range of  $(^{187}\text{Os}/^{188}\text{Os})_i$  values with a 0.8% error suggests that the small-scale variability in this core reflects small changes in the balance of radiogenic versus non-radiogenic  $(^{187}\text{Os}/^{188}\text{Os})_i$  contribution to seawater in the Santa Maria Basin.

The relationship between Re and TOC and Os and TOC correlates well and shows how  $^{187}\text{Re}$ - $^{187}\text{Os}$  isotope systematics can be used to determine depositional environment. The high correlation between Re, Os and TOC for all facies suggests that Re and Os fully complexed in organic matter and supports prior depositional environment studies, such as Wright (2015). Prior

work on the phosphatic-carbonate facies from MacKinnon (1989) shows that it was deposited in a near-shore basin during a time of less restriction, high carbonate productivity, and possessed a large oxygen minimum zone with relatively high sea level compared to the siliceous-shale facies. These factors, combined with little terrigenous input, enabled significant organic matter preservation. The higher slope of TOC versus Os for the phosphatic-carbonate reinforced that it was deposited in an open marine, less restricted environment. The siliceous-shale was deposited during a time of relatively lower sea level than the phosphatic-carbonate facies with more basinal restriction, which the lower slope of TOC versus Os also supports. Rock-Eval data of this Monterey Fm. section identified the kerogen of this study's samples as Type I, also reinforcing the basinal and lacustrine nature reported of the Monterey Fm. (Curiale and Odermatt, 1989; Odermatt and Curiale, 1991; Mackinnon, 1989; Isaacs, 1992).

One early goal of this study was to evaluate the  $(^{187}\text{Os}/^{188}\text{Os})_i$  in conjunction with small-scale stratigraphy and see what if there are any changes with depth. It appears that this study's interval of approximately 350 feet may be too small to capture  $(^{187}\text{Os}/^{188}\text{Os})_i$  variability in the mid-Miocene, or perhaps the section is stratigraphically above or below the Columbia River LIP and Nördinger Ries meteor impact. Larger scale stratigraphic studies could better constrain the  $(^{187}\text{Os}/^{188}\text{Os})_i$  and  $^{187}\text{Re}$ - $^{187}\text{Os}$  isotope systematics of these events. Also, tying  $^{87}\text{Re}$ - $^{187}\text{Os}$  isotope systematics to a contact with a known age such as the Monterey Zone 4 or Zone 5 tuff across multiple cores could provide a larger  $(^{187}\text{Os}/^{188}\text{Os})_i$  variation in supporting geochronologic and environmental context for the Monterey Fm.

## References

- Baioumy H.M., Eglinton L.B., and Peucker-Ehrenbrink B. (2011). Rhenium-osmium isotope and platinum group element systematics of marine vs. non-marine organic rich sediments and coals from Egypt. *Chemical Geology* 285, 70-81.
- Behl, R.J. (2012). Depositional and sedimentologic framework for the Miocene Monterey Fm., CA, in Schwalbach & Behl, (compilers) Monterey Fm Seminar & Core Workshop, AAPG Long Beach, Pacific Coast SEPM & Coast Geol Soc, pp 3-11.
- Birck, J.L., Roy-Barman, M. & Capmas, F. (1997). Re-Os isotopic measurements at the femtomole level in natural samples. *Geostandards Newsletter*, 21, 19-27.
- Brandon A.D., Norman M.D., Walker R.J. and Morgan J.W. (1999).  $^{186}\text{Os}$ - $^{187}\text{Os}$  systematics of Hawaiian picrites. *Earth and Planetary Science Letters* 174, 25-42.
- Burton K.W., Bourdon B., Birck J.-L., Allegre C.J. and Hein J.R. (1999). Osmium isotope variations in the oceans recorded by Fe-Mn crusts. *Earth and Planetary Science Letters* 171, 185-197.
- Cohen, A. , Waters, F.G. (1996). Separation of osmium from geological materials by solvent extraction for analysis by thermal ionisation mass spectrometry. *Analytica Chimica Acta*, 332, 269-275.
- Cohen, A.S., Coe, A.L., Bartlett, J.M., & Hawkesworth, C.J. (1999). Precise Re-Os ages of organic-rich mud rocks and the Os isotope composition of Jurassic seawater. *Earth and Planetary Science Letters*, 167, 159-173.
- Cohen A.S. (2004). The rhenium-osmium isotope system: applications to geochronological and palaeoenvironmental problems. *Journal of the Geological Society of London* 161, 729-734.
- Colodner, D., Sachs, J., Ravizza, G., Turekian, K., Edmond, J., Boyle, E., (1993). The geochemical cycles of rhenium: a reconnaissance. *Earth Planet. Sci. Lett.* 117, 205–221.
- Courtillot, V.E., Renne, P.R., (2003). On the ages of flood basalt events. *C. R. Geosci.* 335 (1), 113–140.
- Creaser, R.A., Papanastassiou, D.A. & Wasserburg, G.J. (1991). Negative thermal ion mass spectrometry of osmium, rhenium, and iridium. *Geochimica et Cosmochimica Acta*, 55, 397-401.
- Creaser, R.A., Sannigrahi, P., Chacko, T. & Selby, D. (2002). Further evaluation of the Re-Os geochronometer in organic-rich sedimentary rocks: A test of hydrocarbon maturation effects in the Exshaw Formation, Western Canada Sedimentary Basin. *Geochimica et Cosmochimica Acta*, 66, 3441-3452.

- Crusius, J., Calvert, S., Pedersen, T., Sage, D., (1996). Rhenium and molybdenum enrichments in sediments as indicators of oxic, suboxic and sulfidic conditions of deposition. *Earth Planet. Sci. Lett.* 145, 65–78.
- Crusius J., Thompson J. (2000). Comparative behavior of authigenic Re, U, and Mo during reoxidation and subsequent long-term burial in marine sediments. *Geochimica et Cosmochimica Acta* 64, 2233-2242.
- Cumming, V.M., Selby, D., Lillis, P.G., (2012). Re-Os geochronology of the lacustrine Green River Formation: Insights into direct depositional dating of lacustrine successions, Re-Os systematics and paleocontinental weathering. *Earth Planet. Sci. Lett.* 359, 194-205
- Curiale, J., Odermatt, J.R. (1989). Short Term biomarker variability in the Monterey Formation, Santa Maria Basin. *Organic Geochemistry*, 14.1, 1-13.
- Demaison, G.J., Moore, G.T., (1980). Anoxic environments and oil source bed genesis. *Org. Geochem.* 2, 9–31.
- Dibblee, Jr., T. W. (1950). Geology of Southwestern Santa Barbara County, California, Point Arguello, Lompoc, Point Conception, Los Olivos, and Gaviota Quadrangles. State of California Division of Mines, 50, 1-90.
- Durham, L. (2010). Monterey Shale Gets New Look. *AAPG Explorer*, 31, 10-12.
- Esser B.K., Turekian K.K. (1988). Accretion rate of extraterrestrial particles determined from osmium isotope systematics of Pacific pelagic clay and manganese nodules. *Geochimica et Cosmochimica Acta* 52, 1383-1388.
- Esser B.K., Turekian K.K. (1993). The osmium isotopic compositions of the continental crust. *Geochimica et Cosmochimica Acta* 57, 3093-3104.
- Georgiev S., Stein H.J., Hannah J.L., Bingen B., Weiss H.M. and Piasecki S. (2011). Hot acidic Late Permian seas stifle life in record time. *Earth and Planetary Science Letters* 310, 389-400.
- Gradstein, F.M., Ogg, J.G., (2012). The Geologic Time Scale, Chapter Two, The chronostratigraphic time scale. Elsevier Publishing. 31-42.
- Gramlich J.W., Murphy T.J., Garner E.L. and Shields W.R. (1973). Absolute isotopic abundance ratio and atomic weight of a reference sample of rhenium. *Journal of Research of the National Bureau of Standards* 77A, 691-698.
- Hart S.R., Ravizza G. (1996). Os partitioning between phases in lherzolite and basalt in earth processes: reading the isotopic code. *AGU Geophysical Monograph*.
- Herzberg C.T. (1993). Lithosphere peridotites of the Kaapvaal Craton. *Earth and Planetary Science Letters* 120, 13-29.

- Hirt B., Tilton G.R., Herr W. and Hoffmeister W., (1963). The half-life of  $^{187}\text{Re}$ . In: Geiss J. and Goldberg E. (Eds.), *Earth Science and Meteoritics*, North Holland, Amsterdam.
- Horan, M.F., Morgan, J.W., Grauch, R.I., Coveney Jr., R.M., Murowchick, J.B. & Hulbert, L.J. (1994). Rhenium and osmium isotopes in black shales and Ni-Mo-PGE-rich sulfide layers, Yukon Territory, Canada, and Hunan and Guizhou provinces, China. *Geochimica et Cosmochimica Acta*, 58, 257-265.
- Hornafius, J.S., (1994). Field guide to the Monterey Formation between Santa Barbara and Gaviota, California. AAPG Field Guide.
- Ibach, L.E.J., (1982). Relationship between sedimentation-rate and total organic carbon content in ancient marine-sediments. *AAPG Bull. Am. Assoc. Pet. Geol.* 66, 170–188.
- Isaacs, C. M. (1992). Preliminary petroleum geology background and well data for oil samples in the cooperative Monterey organic geochemistry study, Santa Maria and Santa Barbara-Ventura Basins, California. U.S. Geological Survey, Report 92-539-F,1-42.
- Kendall, B. S., Creaser, R. A., Ross, G. M., Selby, D. (2004). Constraints on the timing of Marinoan ‘Snowball Earth’ glaciation by  $^{187}\text{Re} - ^{187}\text{Os}$  dating of a Neoproterozoic post-glacial black shale in Western Canada. *Earth and Planetary Science Letters*, 222, 729-740.
- Kendall, B., Creaser, R.A., Selby, D., (2009).  $^{187}\text{Re}-^{187}\text{Os}$  geochronology of Precambrian organic-rich sedimentary rocks. *Geological Society*, 326. Special Publications, London, pp. 85–107.
- Klemm, V., Frank, M., Levasseur, S., Halliday, A.N., Hein, J.R., (2008). Seawater osmium isotope evidence for a middle Miocene flood basalt event in ferromanganese crust records. *Earth and Planetary Science Letters*, 273, 175-183.
- Koide, M., Goldberg, E.D., Niemeyer, S., Gerlach, D., Hodge, V., Bertine, K.K., Padova, A., (1991). Osmium in marine sediments. *Geochem. Cosmochem. Acta* 55, 1641–1648.
- LeFever, J.A., Martiniuk, C.D., Dancsok, E.F.R. & Mahnic, P.A. (1991). Petroleum potential of the middle member of the Bakken formation, Williston basin, in J.E. Christopher and F.M. Haidl, eds., 6th International Williston basin symposium. *Saskatchewan Geological Society Special Publication*, 11, 74-94.
- Levasseur, S., Birck, J., Allegre, C.J., (1998). Direct measurement of femtomoles of osmium and the  $^{187}\text{Os}/^{186}\text{Os}$  ratio in seawater. *Science* 282, 272–274.
- Luck J.M., Birck J.L., Allegre C.J. (1980).  $^{187}\text{Re}-^{187}\text{Os}$  systematics in meteorites: early chronology of the solar system and age of the galaxy. *Nature* 283, 256-259.

- Luck J.M., Allegre C.J. (1982). The study of molybdenites through the  $^{187}\text{Re}$ - $^{187}\text{Os}$  chronometer. *Earth and Planetary Science Letters* 61, 291-296.
- Luck J.M., Allegre C.J. (1983)  $^{187}\text{Re}$ - $^{187}\text{Os}$  systematics in meteorites and cosmochemical consequences. *Nature* 302, 130-132.
- Ludwig, K., (2008). Isoplot, version 4.0: a geochronological toolkit for Microsoft Excel. Berkeley Geochronology Centre Special Publication no. 4.
- Mackinnon, T., (1989). Oil in the California Monterey Formation. American Geophysical Union Field Trip Guidebook
- McArthur, J.M., Algeo, T.J., van de Schootbrugge, B., Li, Q., Howarth, R.J., (2008). Basinal restriction, black shales, Re–Os dating, and the Early Toarcian (Jurassic) oceanic anoxic event. *Paleoceanography* 23 (4), PA4217.
- Miller C.A. (2004). Re–Os dating of algal laminites: reduction-enrichment of metals in the sedimentary environment and evidence for new geoporphyryns. MSc Thesis, University of Saskatchewan, Saskatoon, Canada.
- Montanari, A., Koeberl, C., (2000). Impact Stratigraphy, the Italian Record. Lecture Notes in Earth Sciences. Springer Verlag, p. 93.
- Morford, J.L., Emerson, S., (1999). The geochemistry of redox sensitive trace metals in sediments. *Geochem. Cosmochem. Acta* 63, 1735–1750.
- Nicholson, C., Sorlien, C.C., Luyendyk, B.P. (1992). Deep crustal structure and tectonics in the offshore southern Santa Maria Basin, California. *Geology*, 20, 239-242.
- Odermatt, J.R., Curiale J.A. (1991). Organically Bound Metals and Biomarkers in the Monterey Formation of the Santa Maria Basin, California. *Chemical Geology*, 91, 99-113.
- Peucker-Ehrinbrink B., Ravizza G. and Hoffmann A.W. (1995). The marine  $^{187}\text{Os}/^{188}\text{Os}$  record of the past 80 million years. *Earth and Planetary Science Letters* 130, 155- 176.
- Peucker-Ehrenbrink B., Ravizza G. (2000). The marine osmium isotope record. *Terra Nova* 12, 205-219.
- Peucker-Ehrenbrink, B., Ravizza, G. (2012). Osmium Isotope Stratigraphy. *The Geologic Time Scale*, Ch. 8. 145-166
- Pisciotta, K.A., Garrison, R.E. (1981). Lithofacies and depositional environments of the Monterey Formation, California. *The Monterey Formation and related Siliceous Rocks of California*, Pacific Section, Soc. Econ. Paleontologists and Mineralogists, p. 97-122.
- Poirier, A., Hillaire-Marcel, C., (2011). Improved Os-isotope stratigraphy of the Arctic Ocean. *Geophys. Res. Lett.* 38, L14607.

- Ravizza, G. & Turekian, K.K. (1989). Application of the  $^{187}\text{Re}$ - $^{187}\text{Os}$  system to black shale geochronometry. *Geochimica et Cosmochimica Acta*, 53, 3257-3262.
- Ravizza G. (1993). Variations of the  $^{187}\text{Os}/^{186}\text{Os}$  seawater over the past 28 million years as inferred from metalliferous carbonates. *Earth and Planetary Science Letters*, 118, 335-348.
- Reusch, D., Ravizza, G., Maasch, K., Wright, J., (1998). Miocene seawater  $^{187}\text{Os}/^{188}\text{Os}$  ratios inferred from metalliferous carbonates. *Earth and Planetary Science Letters* 160, 163-178.
- Rooney A.D., Selby D., Houzay J.-P. and Renne P.R. (2010). Re-Os geochronology of a Mesoproterozoic sedimentary succession, Taoudeni Basin, Mauritania: Implications for basin-wide correlations and Re-Os organic-rich sediments systematics. *Earth and Planetary Science Letters* 289, 486-496.
- Rooney A.D., Selby D., Lewan M.D., Lillis P.G. and Houzay J.-P. (2012). Evaluating ReOs systematics in organic-rich sedimentary rocks in response to petroleum generation using hydrous pyrolysis experiments. *Geochimica et Cosmochimica Acta* 77, 275-291.
- Schmidt, G., Pernicka, E., 1994. The determination of platinum-group elements (Pge) in target rocks and fall-back material of the Nordlinger Ries Impact Crater, Germany. *Geochim. Cosmochim. Acta* 58 (22), 5083–5090.
- Schwalbach, J.R., Bohacs, K.M., (1992). *Sequence Stratigraphy in Fine-Grained Rocks: Examples from the Monterey Formation*. Society for Sedimentary Geology, Pacific Section Field Trip Guide.
- Selby, D., and Creaser, R.A. (2003). Re-Os geochronology of organic rich sediments: an evaluation of organic matter analysis methods. *Chemical Geology*, 200, 225-240.
- Selby, D., Creaser, R.A., (2005). Direct radiometric dating of the Devonian– Mississippian time-scale boundary using the Re–Os black shale geochronometer. *Geology* 33, 545–548.
- Selby, D., Mutterlose, J., Condon, D.J., (2009). U–Pb and Re–Os geochronology of the Aptian/Albian and Cenomanian/Turonian stage boundaries: implications for timescale calibration, osmium isotope seawater composition and Re–Os systematics in organic-rich sediments. *Chem. Geol.* 265, 394–409.
- Shirey, S.B. & Walker, R.J. (1995). Carius Tube Digestion for Low-Blank Rhenium-Osmium Analysis. *Analytical Chemistry*, 67, 2136-2141.
- Smoliar, M.I., Walker, R.J., Morgan, J.W., (1996). Re–Os isotope constraints on the age of Group IIA, IIIA, IVA, and IVB iron meteorites. *Science* 271, 1099–1102.

- Tripathy, G.R., Hannah, J.L., Stein, H.J., Yang, G., (2014). Re-Os age and depositional environment from the Cambrian-Ordovician boundary, Green Point, western Newfoundland. *Geochemistry, Geophysics, Geosystems (AGU) volume 15.4*
- Turgeon, S.C., Creaser, R.A., Algeo, T.J., (2007). Re-Os depositional ages and seawater Os estimates for the Frasnian-Famennian boundary: implications for weathering rates, land plant evolution, and extinction mechanisms. *Earth Planet. Sci. Lett.* 261, 649–661.
- Volkening, J., Walczyk, T. & Heumann, K.G. (1991). Osmium isotope ratio determinations by negative thermal ionization mass spectrometry. *International Journal of Mass Spectrometry and Ion Processes*, 105, 147-159.
- Walker R.J., Carlson R.W., Shirey S.B. and Boyd F.R. (1989). Os, Sr, Nd, and Pb isotope systematics of southern Africa peridotite xenoliths: Implications for the chemical evolution of subcontinental mantle. *Geochimica et Cosmochimica Acta* 53, 1583- 1595.
- Walker R.J., Morgan J.W., Horan M.F., Czamanske G.K., Krogstad E.J., Fedorenko V.A. and Kuniylov V.W. (1994). Re-Os isotope evidence for an enriched-mantle source for the Norilsk-type ore-bearing intrusions, Siberia. *Geochimica et Cosmochimica Acta* 58, 4179-4197.
- Wright, S.W., (2015). Applications of the Rhenium-Osmium System and Platinum and Iridium Abundances in Organic-Rich Mud rocks: A Geochronology, Geochemistry, and Redox Study. PhD Dissertation.
- Yamashita Y., Takahashi Y., Haba H., Enomoto S. and Shimizu H. (2007). Comparison of reductive accumulation of Re and Os in seawater-sediment systems. *Geochimica et Cosmochimica Acta* 71, 3458-3475.
- York D. (1969). Least-squares fitting of a straight line with correlated errors. *Earth and Planetary Science Letters* 5, 320-324.